Turkish Journal of Electromechanics and Energy

an international, open access journal

SL PUBLISHING Science Literature

www.scienceliterature.com

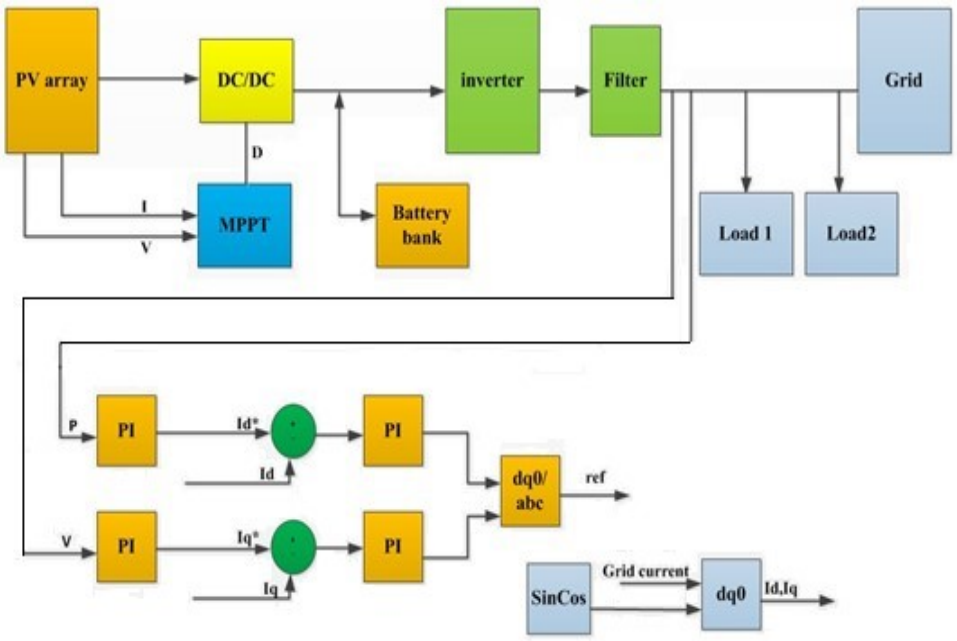

TURKISH JOURNAL OF ELECTROMECHANICS AND ENERGY

VOLUME 3 NO 2

ISSN 2547-975X

July-December 2018 issue

Modified P&O Technique for Hybrid PV-Battery-Smart Grid Integrated Scheme
Mohamed Salama EBRAHİM, Adel Mahmoud SHARAF, Ahmed Mohamed ATALLAH, Adel Sedky EMARAH
pp. 1-7

Control of Fuel Cells-Electric Vehicle Based on Direct Torque Control
Djamila REKIOUA, Zahra MOKRANİ, Toufik REKİOUA
pp. 8-14

Photovoltaic Parameters Estimation Using Hybrid Flower Pollination with Clonal Selection Algorithm
Ahmed Kamal RYAD, Ahmed Mohamed ATALLAH, Abdelhaliem ZEKRY
pp. 15-21

Estimation of Voltage Profile and Short-Circuit Currents for a Real Substation Distribution System
Alkan AKSOY, Fatih Mehmet NUROĞLU
pp. 22-27

SCIENCE LITERATURE

Kazım Karabekir Business-Center, F:3/C/196, 50. Year Street, Lalapaşa Neighborhood, Yakutiye, Erzurum, Turkey

https://www.scienceliterature.com

01.12.2018

Research Article | Submit Manuscript

Turkish Journal of Electromechanics & Energy

ISSN-2547-975X

Modified P&O Technique for Hybrid PV-Battery Smart Grid Integrated Scheme

Mohamed S. Ebrahim[1*], Adel M. Sharaf[2], Ahmed M. Atallah [3], Adel S. Emarah[3]

[1]Turbo-machinery Division, Shell Gas Company, Cairo, Egypt
[2] Senior, Life Member of IEEE, Fredericton, NB, Canada
[3] Electrical Power & Machine Department, Ain Shams University, Cairo, Egypt

Received: 6 March 2018; Revised: 20 April 2018; Accepted: 13 June 2018; Published: 1 December 2018

Turk J Electrom Energ Vol.: 3 No: 2 Page: 1-7 (2018)

SLOI: http://www.sloi.org/

*Correspondence E-mail: engmohamed_24@yahoo.com

ABSTRACT This paper presents a PV-Battery smart grid photovoltaic system through use of a modified perturbs and observes (P&O) technique for energy efficient utilization and ensuring the maximum power point tracking (MPPT). The modified P&O is based on step by step power-change in the specified three distinct search zones using an assigned zone- duty cycle ratio of the chopper converter (D). The PV-Battery-smart grid integrated system utilized a proportional integral (PI) controller for Li-Ion battery charging with a feed forward battery current signal for fast charging. LC filter is used to reduce current ripple introduced by PWM switching and modulating of the grid-side voltage source inverter (VSI). Digital simulation results using the MATLAB/Simulink software environment validated the effectiveness of the proposed control scheme for efficient energy utilization and reduced ripple contents in the DC and AC side of the VSI-inverter as well as it provided fast battery charging.

Keywords: PV-Battery-Smart Grid, Modified P&O, Maximum Power Tracking, Fast Charging

Cite this article: M. S. Ebrahim, A. M. Sharaf, A. M. Atallah, A. S. Emarah, Modified P&O Technique for Hybrid PV-Battery Smart Grid Integrated Scheme, Turkish Journal of Electromechanics & Energy 3(2) 1-7 (2018).

1. INTRODUCTION

Renewable energy resources (solar, wind, tidal, wave etc.) are increasingly considered as viable and economic alternative sources to the electric utility-generation mix. Conventional fossil-fuel energy sources are declining with increased use, population growth, growing concerns over gaseous emission and global warming. Photovoltaic (PV) array is considered to be promising power source in future low carbon electric grid. Photovoltaic arrays are subject to variations in power/energy output due to variations in insolation/irradiation and operating temperatures. One effective technique is to add multi-source and storage devices such as Li-Ion batteries, fuel cells, super-capacitors and superconductive magnetic energy storage (SMES) systems [1], and battery energy storage systems [2]. The diesel back-up for PV power systems is capable of providing a continuous 24-hours power supply but with low energy efficiency and additional fuel cost of low power output. SMES technology has a significant potential health risk due to strong ambient magnetic fields. The battery storage systems are considered a common way to store energy when the main source of power is sufficient to provide energy in case of light loads. Power electronic conversion devices are required for both DC and AC interface such as inverter and DC-DC converter. One of the main tasks of these devices is to continuously adapt the hybrid DC-AC interface system to ensure power matching between generation and load while ensuring the maximum power utilization from the PV array under varying weather and load conditions. Nonlinear characteristic of a PV power curve is a function of the irradiance level and temperature [4], for best efficient energy utilization it is necessary to operate the system at its Maximum Power Operating Condition MPP.

There are several methods used to achieve the maximum power tracking and efficient energy utilization. One of which is perturb and observe method (P&O) [5]. It is the most common method and widely adopted. Perturb and observe method has simple implementation yet it has drawbacks where the perturbation process will lead the operation point of the PV array to oscillate around the maximum power point (MPP). Secondly, the P&O method probably fails to track the MPP when the insolation level changes rapidly [5]. Incremental conductance (IC) method offers good

performance under the rapidly changing conditions in insolation [6]. Regulation controllers require high sampling and fast dynamics to cope with sudden load excursions and variations in insolation/irradiation and operating temperatures. PV-Battery-Smart Grid interconnected schemes have two control loops. The first loop is a pulse width modulation (PWM), which regulates the output currents of the VSI-inverter, to meet the requirements of the waveform and phase. The second loop is to control the output power of the inverter based on MPP-maximum PV search. Both regulators use a two-stage tiered power conversion [7].

This paper deals with power/energy optimized management for a PV-Battery interfaced to smart grid, modified P&O is used to achieve MPPT under changes in weather conditions. The battery system is connected to the PV array and charging of the output power from the DC/DC converter. A new algorithm of charging controller is used to control the charging process through the PI controller with feed forward from the battery current. In addition, the power flow from PV- hybrid system is connected to the grid and controlled through a PI controller. The next section details the structure of the unified system components which comprised of PV, battery, filter capacitors and interface VSI-to smart grid system. The MPPT search was achieved using the modified P&O search algorithm. PI controller with battery current feedback is used for battery charging. Third section presents the structure of MPPT, where the goal of MPPT system is to provide a fixed input voltage and - or current to reach the maximum power point (MPP). Forth section presents the efficient battery charging controller to regulate the DC voltage. Fifth section presents the optimization algorithm for efficient energy exchange. Dynamic simulation results and conclusions are presented in sections 6 and 7, respectively.

2. PROPOSED SYSTEM

The block diagram that represents the proposed system is shown in Figure 1**.**

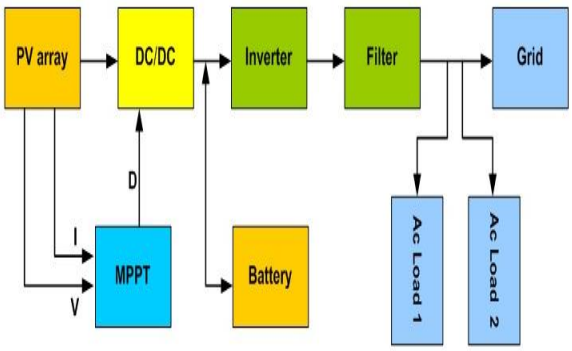

Fig. 1. Integrated PV-Battery- Inverter-Smart grid system

Figure 1 shows the schematic of the PV (11 kW) unified system with key subsystems. The PV is feeding the load (load 1 is 5 kW & 1 kVAr, load 2 is 3 kW & 1 kVAr) and ensures continuous charges the battery through a buck DC-DC chopper converter using the maximum power point tracking (MPPT) algorithm. The DC-DC converter is controlled by a PWM using modified P&O. The battery is continuously connected to the common voltage bus, through an additional DC-DC converter. The power may flow through the battery in both directions. The charging current is regulated by controlling the bus voltage. VSI-Inverter is used to provide the required AC power to the AC side loads.

3. POWER CONTROL OF PHOTOVOLTAIC SYSTEM

P&O algorithm shown in Figure 2 is preferred in industrial applications, due to its simplicity. Many ways are proposed to improve the response of P&O through control the perturbation steps such as modified P&O with fixed perturbation. Modified P&O with adaptive step by step zonal perturbations is proposed to achieve MPPT [5]. A photovoltaic cell has a nonlinear voltage-current characteristic with varying power/energy output due to the change in environmental conditions such as solar insolation level, ambient temperature, and the load.

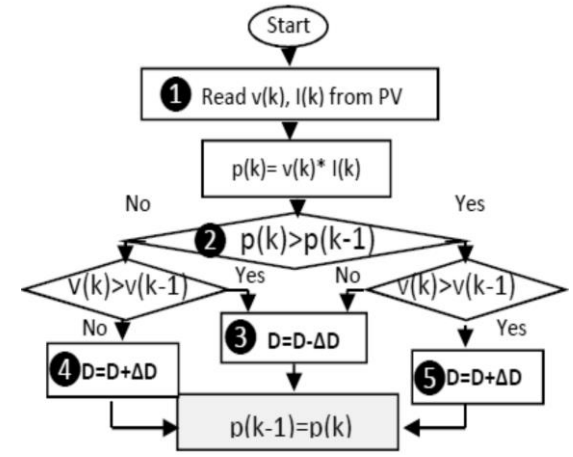

(a)

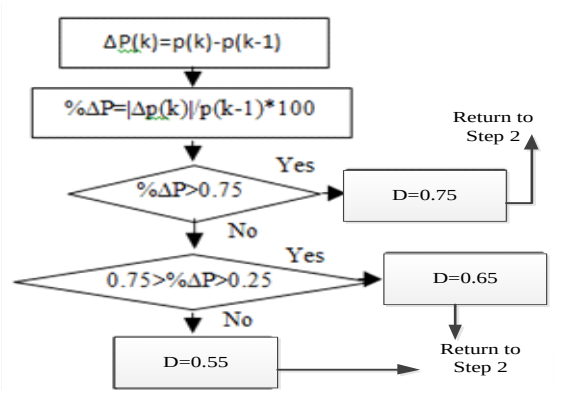

(b)

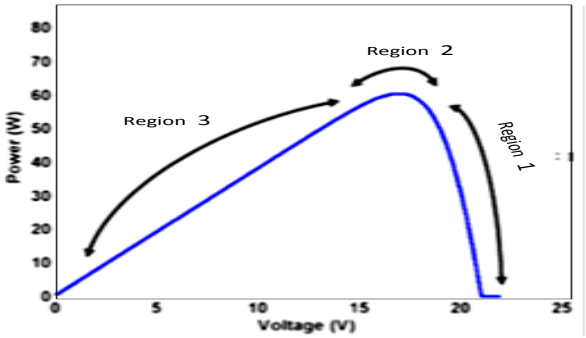

(c)

Fig. 2. (a) The algorithm of perturb and observe (P&O), (b) Proposed of perturb and observer, (c) PV cell (Power/Voltage) curve operating regions

The PV source needs to track the maximum power point (MPP) by controlling a DC-DC converter. This section represents the novel way to achieve MPPT. This proposed algorithm aimed to enhance the dynamic power utilization and increase the efficient operation of the traditional P&O method and eliminates its drawbacks. The modified P&O search algorithm based zonal power levels are scaled for the specified three selected zones. The power change in each zone has pre-assigned zonal-switching duty cycle ratio (D) for the DC-DC converter (chopper) with an initial preset value. Figure 2 represent the schematic diagram of the traditional P&O, search algorithm based on the modified P&O, and power/voltage of the PV system. The control strategy is divided into two parts: the first part deals with Power from the hybrid system "PV-Battery System", and the second part controls the power delivered to AC side using the VSI Inverter.

The criterion proposed in the flowchart of the proposed controller (MPPT) divides the P-V curve into three regions, as shown in Fig 2(c). The three levels of the perturbation step are as follows: D=0.75 for region 3; D= 0.55 for region 2; and D=0.65 suits for region 1.

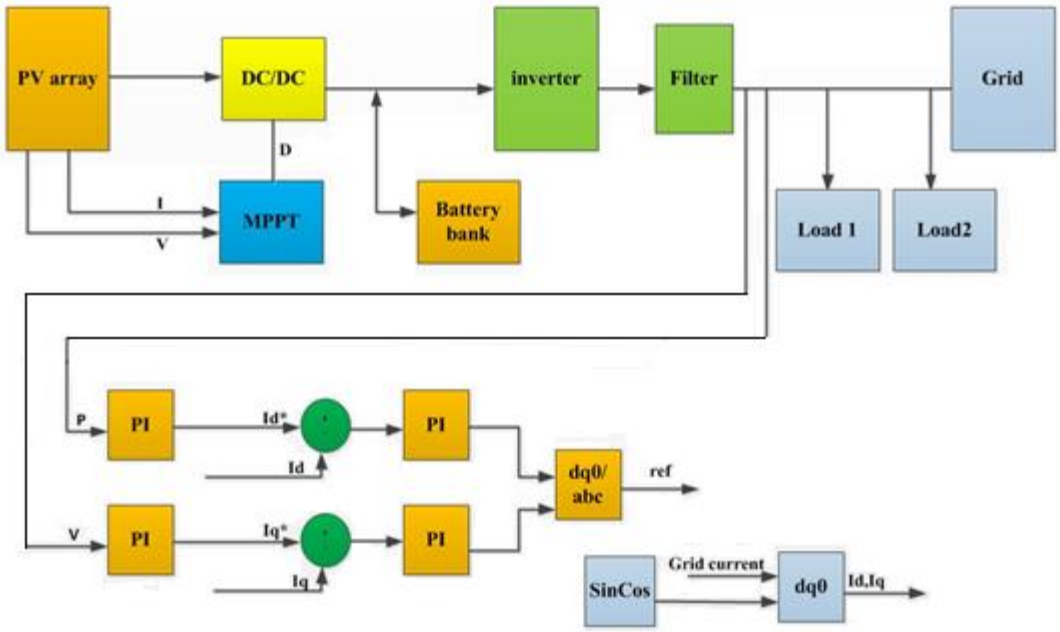

Fig.3. Complete system layout

4. MODIFIED CONTROL STRATEGY

Power from PV array is utilized to feed the load and charging the battery. The weather conditions has a great effects on the output power of the PV array, hence the MPPT is used. To ensure that the value of the DC bus voltage is maintained within the required range, DC-DC converter is used to charge the battery. PI controller is used to control the DC-DC converter, through generating the required duty cycle (D). Feed forward from the battery current (I_b), and the state of charge of the battery (SOC) are considered [6]. From AC side, to simplify the way of the control design for PV grid-connected system, there are many methods of transformation are utilized to reduce the mathematical model of the system [8, 9]. Figure 3 represents the complete system layout. The most common methods of transformations are αβ transformation and d-q transformation (Park transformation). Park's transformation was used in this study. Park's transformation converts a three-phase (A, B, C) into a two-dimensional system (d-q) as αβ transformation is carried out. The differences is appeared in the coordinate, where in αβ the coordinate is stationary, while in Park's transformation the coordinate rotates with a constant frequency. To connect the PV with the grid system, synchronization considered to be the essential part to achieve connection with the grid. To achieve the synchronization, the amplitude and phase value of the grid voltage need to be well known. This information is essential for the voltage and current control loops in order to work at its optimal point. There are various methods used to achieve synchronization with the frame such as zero crossing, phase locked loop (PLL) [10]. PLL was preferred in current study. This algorithm had a better rejection of the harmonic and disturbance compared to zero-crossing [11].

PV systems in the grid required additional functionality from the inverter, such as synchronization, active and reactive power control [12-14]. The control of the inverter is based on a decoupled control of the active and reactive power. The proportional-integral controller (PI) is used to control the output power (P) from the inverter, it provides the active direct current reference (Id*) in a synchronous reference frame. The quadrature component (I_q) that effects on the reactive power is controlled through PI controller. Applying the inverse Park's transformation to d–q frame current vector components, the desired I_{d_ref} &I_{q_ref} a-b-c phase current references were obtained. Each component is passed to a unique PI controller, which outputs the pulses to drive the inverter. Figure 4 represents the structure of system components where the PV array was chosen so that the output voltage of the DC-DC converter suits the inverter's requirements. In this case, a 440V AC grid was chosen, so the requirement for the inverter will be 650V in DC bus to operate properly.

5. DYNAMIC SIMULATION RESULTS

To validate the effectiveness of the proposed control scheme, a step dynamic response of the proposed P&O was examined. The irradiance level was 900W/m². Figure 4 (a) shows the proposed controller that tracks the operating point very quickly. From the battery side, PI battery charging controller is utilized to regulate the DC voltage, through generating the required duty cycle. The output control signal from the control algorithms based on calculating the DC bus voltage with its reference value. Feed forward from the battery current is used to improve the charging response in addition SOC.

Figure 4 (b) represents the response of the DC bus voltage using the battery charging controller. It can be noticed that the DC bus voltage fast conversion to the reference value was achieved when PI controller with DC-DC converter is used. Figure 5 (a), represents the load output power. Figure 5 (b) represents the output power from the voltage source control (VSC), the power from PV array is the same as in Figure 4(a). From the Figure 5 (c), it is observed that when load one is energized the output power from the inverter is higher than the demand power, P_{inv} > PL, then the remaining power feeding into the grid. The load two is energized, then the total power output from the inverter is P_{inv} > PL, but in this case the remaining is less than as compared before. The load was changed (increased), but the power feed into the grid is still. The response for the controller was tested under the partial shadowing. The PV array is subjected to the irradiance level based on the profile levels given in Figure6 (a). The response of battery charging PI controller achieved good tracking for the voltage reference value as compared with direct charging. In addition, active and reactive power are measured at the load (load 1+load 2) to determine the effectiveness of the battery charging controller. Figure 6 (b) depicts active and reactive power at the load with battery controller. Figure6-c shows that load 2 (30 kW as a new value) is increased and the total load changed from 8 kW to be 35 kW, P_{inv} < PL. The grid compensates the remaining required power. Figure 6 (c) shows the battery current when P_{inv}< PL, there is no compensation from the battery. In Figure 7, the power at night is supplied to the load via the battery. Another test was performed under fault conditions on the inverter side, then the load is totally feeding from the grid. Figure 8 (a) shows the power flow from the grid to the load and Figure 8 (b) represents the RMS value of the AC voltage. According to the proposed power flow, there are four scenarios as follows: First priority is to feed the load from PV, if the output power from the PV is much higher than the load power. Secondly is to feed the load from PV system and the grid when the output power from the PV is not sufficient hence, the grid compensates the required power to the load. Third priority is to feed the load from battery bank at night. The last priority is to feed the load from grid in case of no power output from the PV hybrid system or the PV hybrid system is failed. The observation from Figure 9 (a, b & c) and the obtained results show the effect of using an inductive filter not only in the AC side, but also in the DC voltage. One of the major aims to use filtering is to eliminate the harmonics and suppress the undesired. Figure 10 shows the MATLAB/Simulink model with all system components.

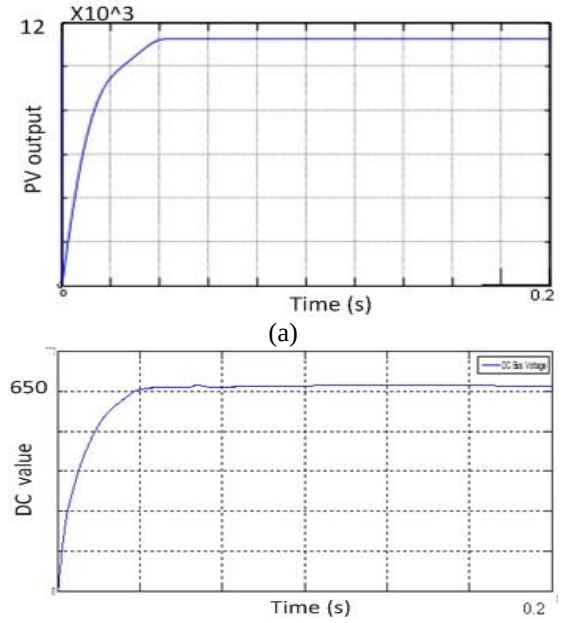

Fig. 4. (a) Output power under irradiance level 900W/m², (b) DC bus voltage

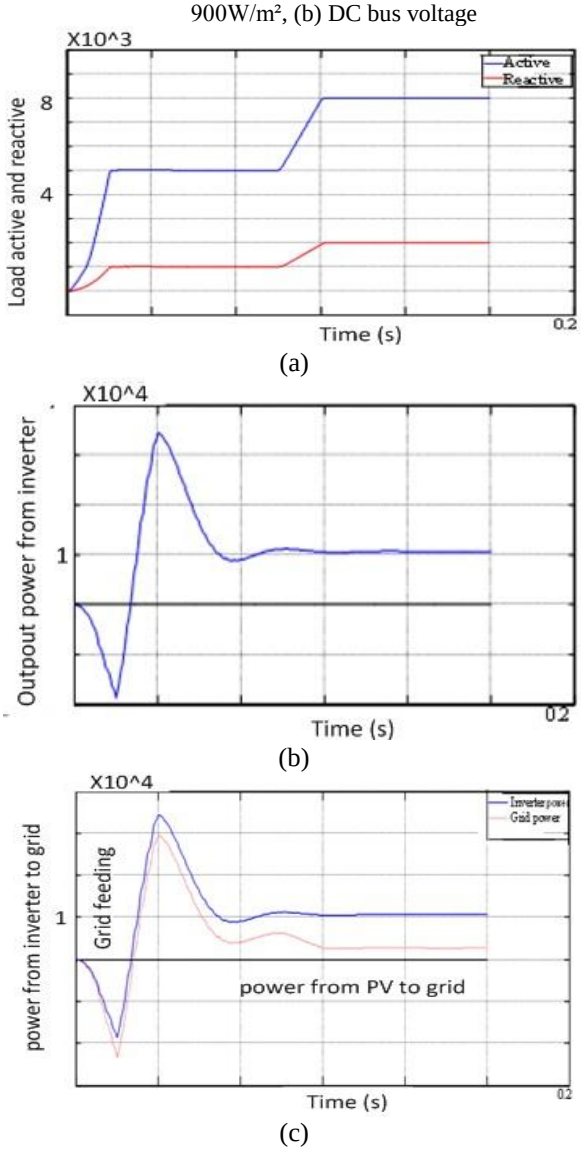

Fig. 5. (a) Load demand power, (b) Inverter output power, (c) Output power from the inverter to grid

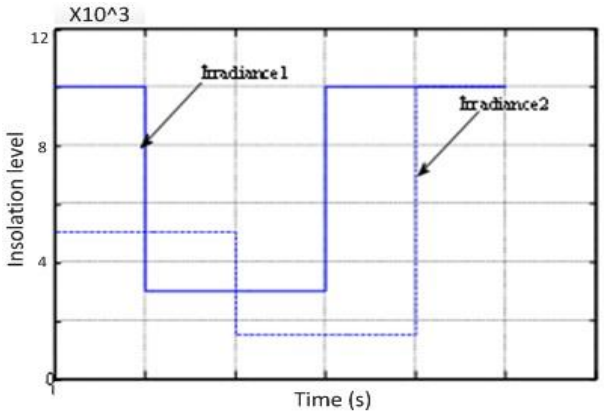

(a)

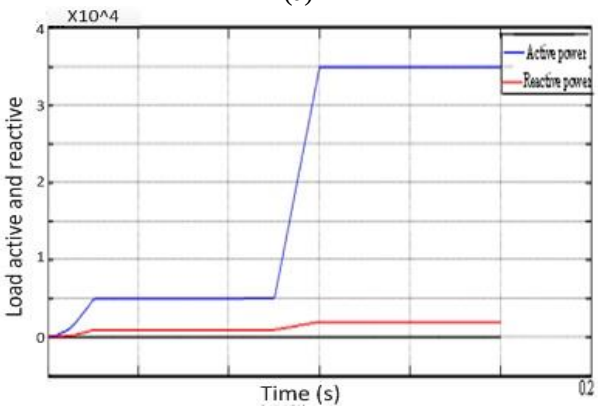

(b)

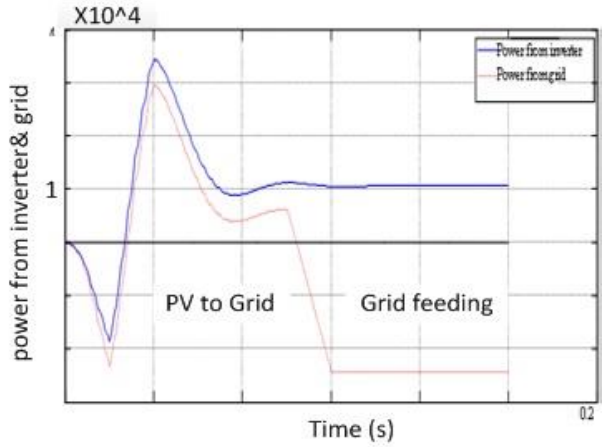

(c)

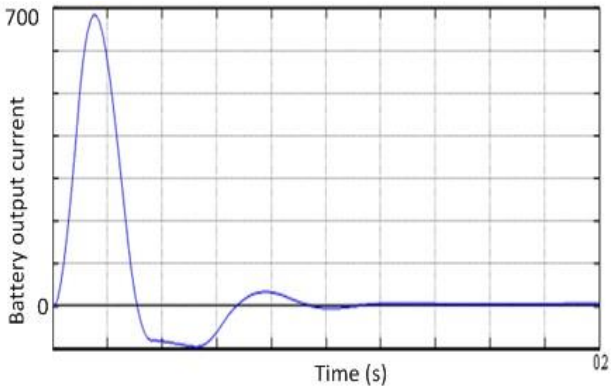

(d)

Fig. 6. (a) Irradiance level, (b) Load demand power, (c) Power from inverter& grid compensation, (d) Battery current when the PL>P_{inv}

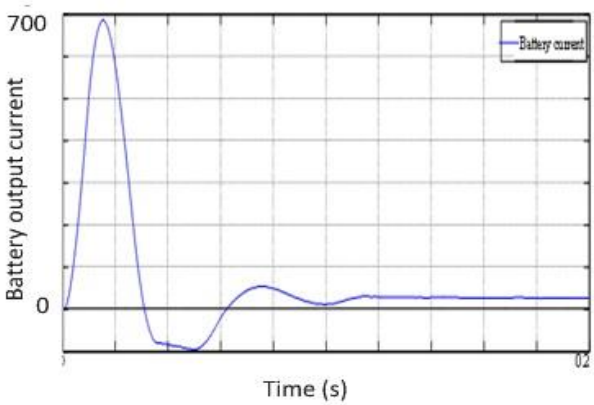

Fig. 7. Battery current during night

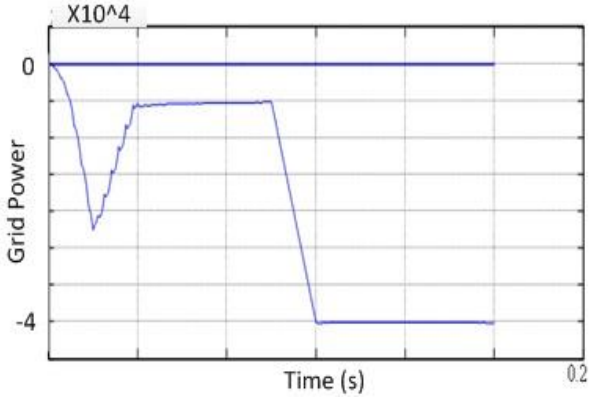

Fig. 8. Power from grid supplied to load

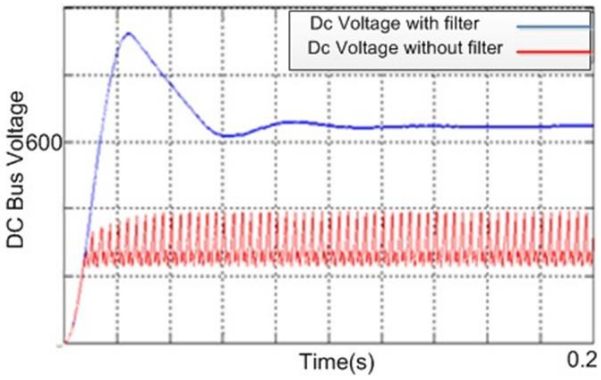

(a)

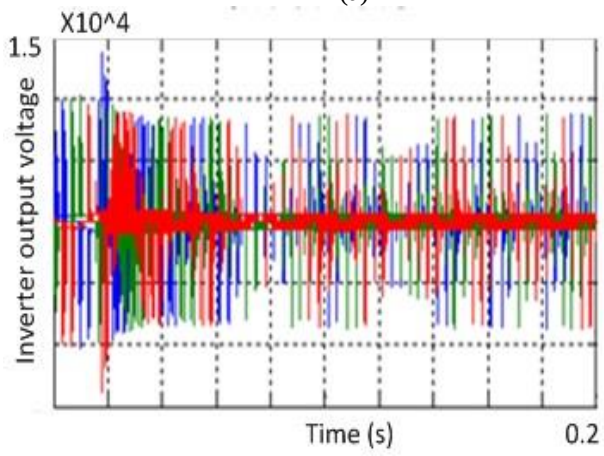

(b)

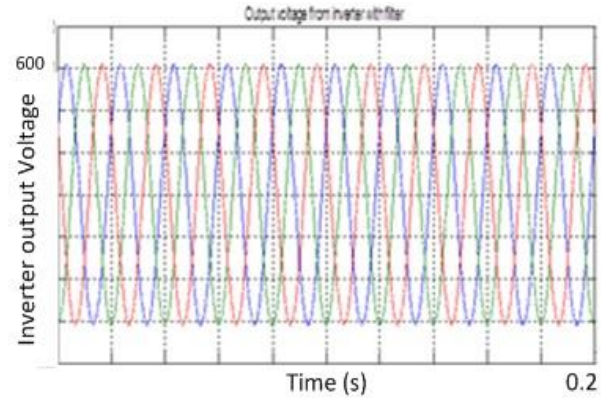

(c)

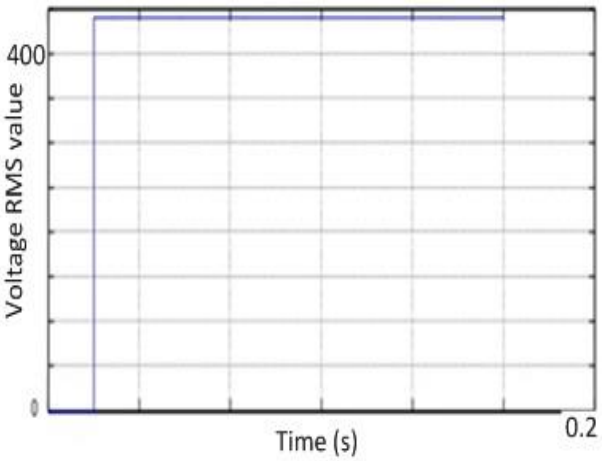

(d)

Fig. 9. (a) Effect of using filter on DC bus voltage, (b) 3Q voltage from inverter without filter, (c) 3Q voltage from inverter when using filter, (d) Voltage RMS value.

6. CONCLUSION

This paper presented a unified integrated PV-Battery-inverter interface to smart grid energy utilization using DC-AC interface. A multi-regulation pulse width modulation (PWM) is switching control scheme using a modified P&O to ensure energy efficient operation. The Modified P&O algorithm is based on multi-zonal pre-specified power change to update duty cycle. The new search algorithm was used to control battery charging with minimal current ripple content through battery current dynamic feedback signal. This is performed using a PI controller combined with feed forward with battery current (I_b). The multi-regulator control scheme for integrated PV-Battery-Inverter fed smart grid with DC and AC side loads are validated for variations in insolation levels, load changes as well as "fault conditions". The integrated scheme with the controllers is validated and assessed for fast dynamic performance, efficient PV solar energy utilization, reduced current ripples as well as fast Li-ion battery continuous charging. An additional LC filter was added to reduce harmonic content and smooth VSI-inverter waveforms at the smart grid interface bus. The inverter control is implemented using Park's transformation with -Phase Locked Loop (PLL) synchronization with AC grid, a second PI controller is used to control the amount of power delivered to the AC side from the VSI-inverter to the smart grid. The modified P&O search and PI controllers for battery charging and decoupled inverter P&Q control will be extended to hybrid PV-Wind-Fuel Cell-Smart Capacitor-Li Ion storage systems, LED lighting schemes and standalone micro grid applications in village/resort/island electricity as well as hydrogen production.

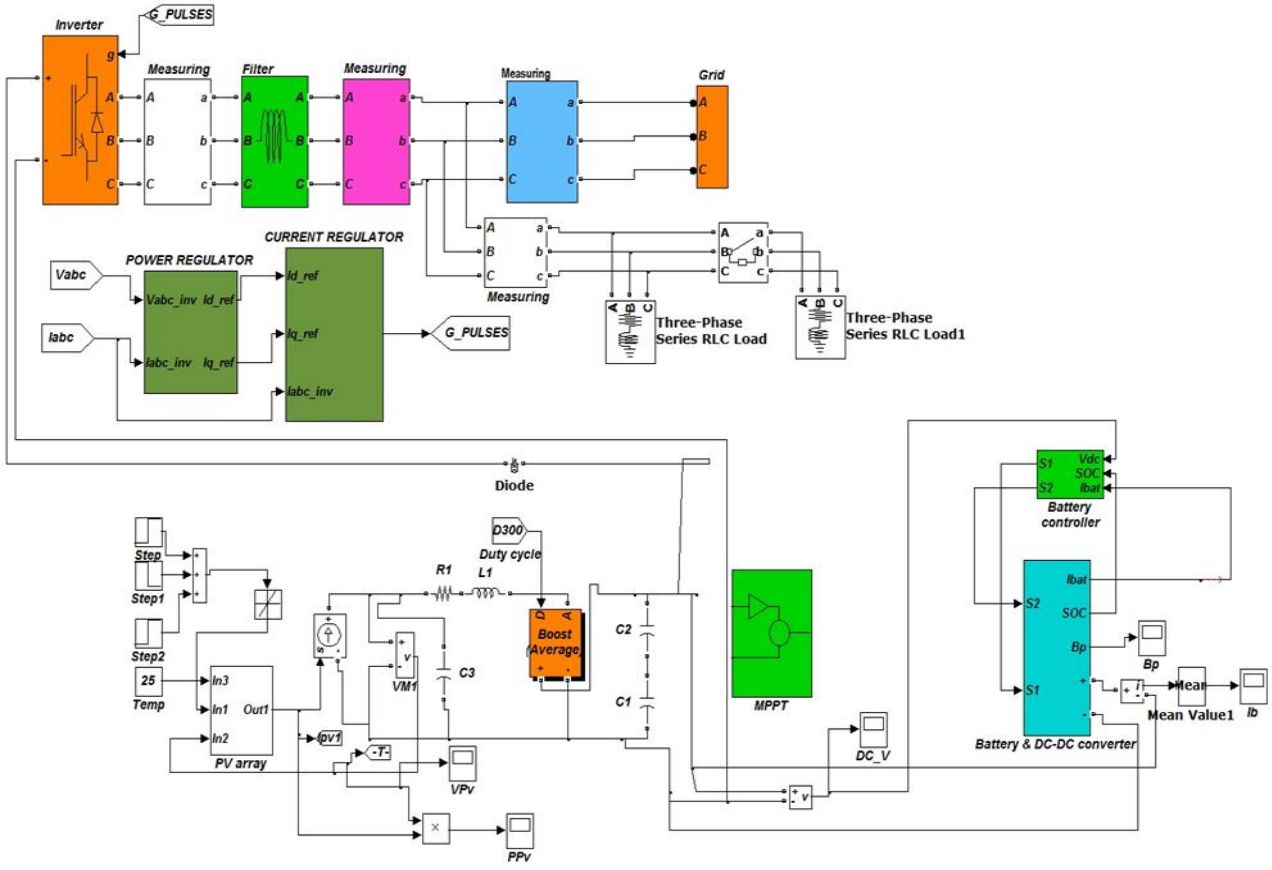

Fig.10. MATLAB/Simulink system model

REFERENCES

[1] T. Zhou, and W. Sun, Study on maximum power point tracking of photovoltaic array in irregular shadow, Electrical Power and Energy Systems, Volume 66, 227-234, (2015).

[2]D. Rekioua, E. Matagne, Optimization of photovoltaic power systems: Modelization, Simulation and Control Green Energy and Technology, 1865-3529, (2012).

[3]A. Mohammedi, D. Rekioua, N. Mezzai, Experimental study of a PV water pumping system Journal of Electrical Systems, 9(2), 212-222, (2013).

[4]M. S. Ebrahim, A. M. Sharaf, A. M. Atallah, and A. S. Emarah, PV solar-optimal maximum power search using a modified P&O technique. EJERS, European Journal of Engineering Research and Science 2(5), (2017).

[5]M. S. Ebrahim, A. M. Sharaf, A. M. Atallah, and A. S. Emarah, An Efficient Controller for Standalone Hybrid- PV Powered System, Turkish Journal of Electromechanics & Energy 2(1), 9-15, (2017).

[6]C. Wang, and M. H. Nehrir, Power Management of a Stand-Alone Wind/Photovoltaic/Fuel Cell Energy System, IEEE Transactions on Energy Conversion, 23(3), 957-967, 2008.

[7] I. A. Aden, H. Kahveci, M. E. Şahin, Single Input, Multiple Output DC-DC Buck Converter for Electric Vehicles, Turkish Journal of Electromechanics & Energy 2(2), 7-13, (2017).

[8] Y. Bo, L. Wuhua, Z. Yi, and H. Xiangning, Design and analysis of a grid connected photovoltaic power system, IEEE Trans. Power Electron., 25(4), 992–1000, (2010).

[9] S. E. Evju, Fundamentals of grid connected photovoltaic power electronic converter design, Ph.D. dissertation, Department of Electrical Power Engineering, Norwegian University of Science and Technology, (2007).

[10] H. Li, Y. Xu, S. Adhikari, D. T. Rizy, F. Li, and P. Irminger UT-Battelle LLC, Tech. Rep, Real and reactive power control of a three-phase single-stage PV system and PV voltage stability, (2012).

[11] F. Blaabjerg, R. Teodorescu, M. Liserre, and A. Timbus, Overview of control and grid synchronization for distributed power generation systems, IEEE Transactions on Industrial Electronics, 53(5), 1398–1409, (2006).

[12] Y. Riffonneau, S. Bacha, F. Barruel, and S. Ploix, Optimal Power Flow Management for Grid Connected PV Systems with Batteries, IEEE Transactions on Sustainable Energy, 2(3), (2011).

[13] B. Lu and M. Shahidehpour, Short term scheduling of battery in a grid connected PV/battery system. IEEE Trans. Power Syst., 20(2), 1053–1061, (2005).

[14] B. Indu Rani, G. S. Ilango, and C. Nagamani, Power flow management algorithm for photovoltaic systems feeding DC/AC loads. Renewable Energy vol.43, 267-275, (2012).

Biographies

Mohamed S. Ebrahim is an electrical and control engineer in Rashpetco-Shell gas plant. He is currently head of the turbo machinery section at the company. He has M.Sc. degree and continue his Ph.D studies. His research areas include renewable energy, and artificial intelligent applications.

Email: Mohamesalama@gmail.com

Prof. Adel M. Sharaf obtained his B.Sc. degree in Electrical Engineering from Cairo University in 1971. He was awarded with M.Sc. degree in Electrical engineering in 1976 and Ph.D. degree in 1979 University of Manitoba, Canada and was employed by Manitoba Hydro as Special Studies Engineer, responsible for engineering and economic feasibility studies in Electrical Distribution System Planning and Expansion. He was selected as NSERC-Canada research-assistant professor in 1980 at University of Manitoba. He joined the University of New Brunswick in 1981 to start a tenure-track academic career as an Assistant professor and he was promoted to Associate Professor in 1983, awarded tenure in 1986, and the full professorship in 1987. He has extensive industrial and consulting experience on electric utilities in Canada and abroad.

E-mail: profdramsharaf@yahoo.ca

Prof. Ahmed M. Atallah earned his B.Sc. and M.Sc. degrees from Electrical Power and Machine Department, Faculty of Engineering, Ain Shams University, Cairo, Egypt, 1979 and 1984, respectively. He was awarded with Ph.D. from Electrical Engineering Department, Faculty of Engineering, University of Alberta, Edmonton, Alberta, Canada, in 1988. His research interest includes renewable energies.

E-mail: ahmed_atallah@eng.asu.edu.eg

Prof. Adel S. Emarah obtained his B.Sc. and M.Sc. from Electrical Power and Machine Department, Faculty of Engineering, Ain Shams University, Cairo, Egypt. 1972 and 1977, respectively. His main research interest is renewable energy technologies.

E-mail: adel_emarah@eng.asu.edu.eg

Research Article | Submit Manuscript

Turkish Journal of Electromechanics & Energy

ISSN-2547-975X

Control of Fuel Cells-Electric Vehicle Based on Direct Torque Control

Z. Mokrani[1], D. Rekioua[1,*], T. Rekioua[1]

[1]Laboratoire LTII, Faculté de Technologie, Université de Bejaia, 06000 Bejaia, Algeria

Received: 4 April 2018; Revised: 6 September 2018; Accepted: 10 October 2018; Published: 1 December 2018

Turk J Electrom Energ Vol.: 3 No: 2 Page: 8-14 (2018)

SLOI: http://www.sloi.org/

*Correspondance E-mail: dja_rekioua@yahoo.fr

ABSTRACT In this paper, proton exchange membrane (PEM) fuel cell electric vehicle is presented as a solution to overcome the alarming pollution problems caused by the conventional internal combustion engine vehicles. To improve the performances of the electric vehicle, the direct torque control (DTC) is applied to the induction machine. It allows us to obtain higher performances with an increasing dependency of the electrical parameters. The use of the PEM fuel cells and the introduction of advanced controls to the DTC results in improved performance of the electric vehicle. The modeling of the whole system is also provided. Obtained results under MATLAB/Simulink was used the compute the performance values of the electric vehicle.

Keywords: Fuel Cell, Electric Vehicle, DTC, Induction Machine

Cite this article: Z. Mokrani, D. Rekioua, T. Rekioua, Control of Fuel Cells-Electric Vehicle Based on Direct Torque Control, Turkish Journal of Electromechanics & Energy, 3(2), 8-14, (2018).

1. INTRODUCTION

Currently, most of the world's energy production comes from fossil energy sources (oil, gas, coal etc.). Excessive consumption of these energy resources, leads to the depletion of these reserves and intensifies the release of greenhouse gases (CO_2, CH_4, etc.) which cause the pollution of the atmosphere. With these alarming consequences, it is necessary to consider the development of alternative energies. Renewable energy sources (wind, solar, biomass, geothermal, hydro etc.) and fuel cell technology are sustainable resources, offering a competitive ecological quality in terms of cost compared to conventional energy sources [1].

The PEM fuel cell is considered as a chemical renewable energy source since it uses H_2 and O_2, which are two abundant chemical elements, to produce energy. A proton exchange membrane fuel cell transforms the chemical energy liberated during the electrochemical reaction of hydrogen and oxygen to electrical energy, as opposed to the direct combustion of hydrogen and oxygen gases to produce thermal energy. The name of chemical source was given due to the reaction which occurs between O_2 and H_2. Output of the reaction is electrical energy, and water.

During the past few years, the fuel cell electric vehicle (EV) gained the interest of industrials, where it is presented as a clean mean of transportation, with no harmful emissions and noise. The development of fuel cell technology offers significant autonomy for the electric vehicle going up to 400-800 km. Most mobile applications and particularly automobiles are dominated by proton exchange membrane fuel cells (PEMFC) [2]. The advantages of the fuel cell allow us to exploit it in the electric vehicle, such as: higher efficiency; silent operation compared to internal combustion engines.

In this context, several studies present the drive of the EV with the fuel cell. Authors studied the electric fuel cell application, the generation of the hydrogen and the integration to the smart city [3-4]. However the control strategy of the electric machine is not addressed. Different types of machines have been used to move EVs. Due to the robustness and low-cost, Induction Motors (IM) have obtained special interests from the industry since their invention. This development allows the introduction of the advanced control, such as Direct Torque Control (DTC), Fuzzy Logic Control (FLC) and Sliding Mode Control (SMC), which are applied to the IMs in order to improve their performances [5-26]. Several researchers employed DTC as reported in literature [5-9, 13-20, 24-25]. In another study, authors used PI and Fuzzy Controller to control induction motor speed [21]. In order to improve performances, some authors have used a combination of several controllers. A combination of DTC and FLC was proposed for IM in [22-23, 26].

In this study, performances analyses of a PEM fuel cells electric vehicle using direct torque control (DTC) are presented. The use of this control method allows us to obtain better performances with an increasing dependency of the electrical parameters. The simulation has been carried out using MATLAB/Simulink.

2. MODELING OF THE PROPOSED SYSTEM

The proposed system is given in Figure 1. It consists principally of an electric vehicle supplied by proton exchange membrane fuel cells (PEMFC) and controlled by DTC control method. Each subsystem has been modeled separately. The electric vehicle has been modeled by an induction motor (IM) fed by an inverter. The global system has been simulated in MATLAB/Simulink.

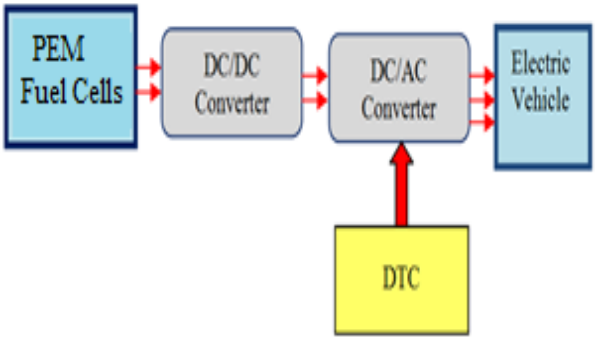

Fig. 1. Proposed PEM fuel cell model

2.1. PEM Fuel Cell Model

A PEMFC is an electrochemical energy converter. The cell voltage V_{PEMFC} is given as the summation of Nernst voltage E_{Nernst} due to various irreversible loss mechanisms, activation overvoltage V_{act}, concentration or diffusion over-voltage V_{conc} and resistive or ohmic over-voltage V_{ohm} as shown in Figure 2 [2, 5, 10, 11].

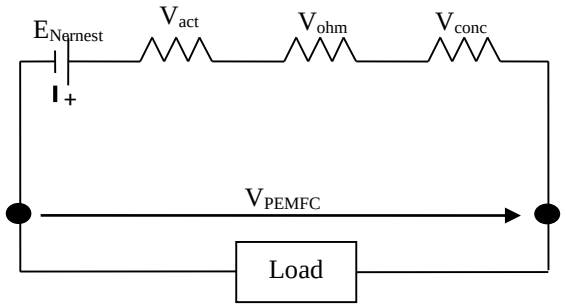

Fig. 2. Electrical representation of a PEMFC

$$V_{PEMFC} = E_{Nernest} - V_{act} - V_{ohm} - V_{conc} \quad (1)$$

$$E_{Nernest} = \alpha_1 + \alpha_2 \times (T_{PEMFC} - 298.15) + \alpha_3 \times T_{PEMFC} \left(0.5 \ln P^*_{O_2} + \ln P^*_{H_2}\right) \quad (2)$$

$$V_{act} = \beta_1 + \beta_2 \times T_{PEMFC} + \beta_3 \times T_{PEMFC} \times \ln\left(j \times 5 \times 10^{-3}\right) + \beta_4 \times T_{PEMFC} \times \ln C^*_{O2} \quad (3)$$

$$V_{ohm} = I_{PEMFC} (R_m + R_c) \quad (4)$$

and

$$R_m = \frac{r_m \times e_m}{S_{cell}} \quad (5)$$

$$V_{conc} = -B \times \ln\left(1 - \frac{j}{j_{max}}\right) \quad (6)$$

where V_{act} is activation overvoltage, V_{conc} is concentration or diffusion over-voltage, V_{ohm} is resistive or ohmic over-voltage, V_{PEMFC} is fuel cell voltage, $E_{Nernest}$ is Nernest voltage, α_i and β_I constants, T_{PEMFC} absolute operating temperature of the stack, P^*_{O2} partial oxygen pressures, P^*_{H2} partial hydrogen pressures, C^*_{O2} oxygen concentration in the cathode area, I_{PEMFC} fuel cell current, j current density, β constant, R_m equivalent resistance of the electron flow, R_c proton resistance, r_m specific resistance of the membrane, e_m thickness of the membrane, S_{cell} membrane active area, λ adjustable parameter in Equation 1 to 6.

Electrical characteristics of PEM fuel cells are represented in Figure 3 and the parameters of the fuel cell used in Equation 2 and 4 are summarized in Table 1.

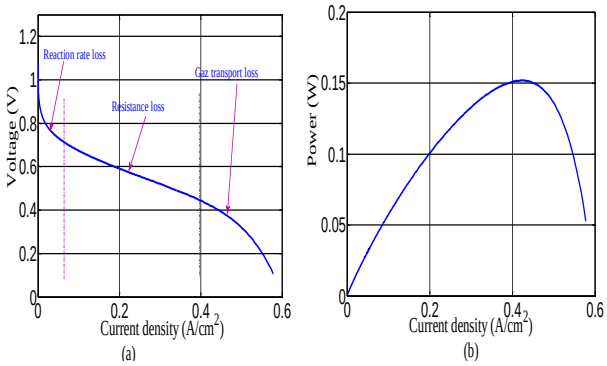

Fig. 3. Voltage characteristic (a), and power characteristic (b)

Table 1. Parameters of the fuel cell

Coefficients	Values
α_1	1.229
α_2	-8.5×10^{-4}
α_3	4.3085×10^{-5}
β_1	-0.9514
β_2	3.12×10^{-3}
β_3	-1.87×10^{-4}
β_4	7.4×10^{-5}

2.2. DC/DC Converter Model

The DC/DC boost converter used is inserted between the source and the inverter. The following equation gives voltage and current expressions of the DC/DC converter [2].

$$\begin{cases} V_{DC} = \dfrac{1}{1-D} V_{FC} \\ I_{DC} = (1-D) I_{FC} \end{cases} \quad (7)$$

2.3. Induction Motor Model

The stator voltage equations can be represented in a stationary reference frame as [1-2, 5, 9]:

$$\begin{cases} V_{s\alpha} = R_{s\alpha} i_{s\alpha} + \dfrac{d\Phi_{s\alpha}}{dt} \\ V_{s\beta} = R_{s\beta} i_{s\beta} + \dfrac{d\Phi_{s\beta}}{dt} \\ V_{r\alpha} = 0 = R_r i_{r\alpha} + \dfrac{d\Phi_{r\alpha}}{dt} - \omega_r \Phi_{r\beta} \\ V_{r\beta} = 0 = R_r i_{r\beta} + \dfrac{d\Phi_{r\beta}}{dt} - \omega_r \Phi_{r\alpha} \end{cases} \quad (8)$$

Equation (9) gives the electromagnetic torque and rotor speed equation:

$$\Gamma_e = \frac{3P}{2}\left(\Phi_{s\alpha} i_{s\beta} - \Phi_{s\beta} i_{s\alpha}\right)$$

$$J \frac{d\Omega}{dt} = \Gamma_e - \Gamma_r \quad (9)$$

Other parameters are listed in Table 2.

Table 2. Parameters of the induction machine

Parameters	*Symbols*	*Values*	*Units*
Shaft power	P_u	3	kW
Nominal speed	N_r	1430	rpm
Frequency	f	50	Hz
Number of pole pairs	P	2	-
Stator resistance	R_s	1.76	Ω
Rotor resistance	R_r	1.95	Ω
Mutual inductance	M	0.183	H
Stator (rotor) self-inductance	L_s=L_r	0.194	H
Moment of Inertia	J	0.02	kg.m^2
Coefficient of viscous friction	f	0.0001	N.m.s/rad

2.4. Methods for Identifying Induction Machine Parameters

Several methods exist to identify machine parameters (such as stator and rotor resistors, stator and rotor cyclic inductances and mutual inductance). We can cite:

- Least squares method (knowledge of partial leakage equivalent scheme and parameter vector).
- Nameplate method, which is a direct method (knowledge of the rated power factor and the model of the machine at steady speed).
- Conventional test method, which is based on the steady-state machine model used in our study.

The steady state phase scheme, also known as coupled inductance scheme, is as shown in Figure 4.

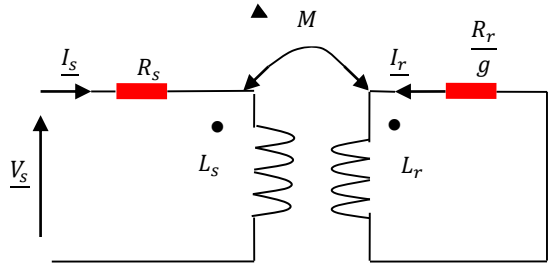

Fig. 4. Steady state phase diagram

$$\underline{V_s} = R_s\underline{I_s} + jL_s\omega_s\underline{I_s} + jM\omega_s\underline{I_r}$$
$$0 = \frac{R_r}{g}\underline{I_r} + jL_r\omega_s\underline{I_s} + jM\omega_s\underline{I_s} \quad (10)$$

We performed the continuous test on one phase to determine the stator resistance R_s of the machine since the inductance term is zero.

The test in synchronism at no load allows us to annul the slip "g'", and we will have as equivalent model of the machine as shown in Figure 5.

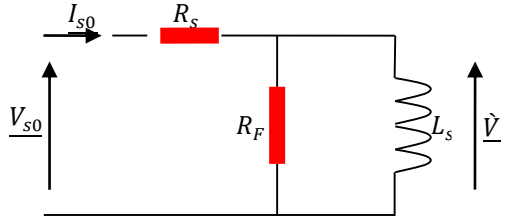

Fig. 5. The equivalent diagram of the machine under synchronism test

No need for these power active P_0 , reactive power $Q_0 = \sqrt{S_0^2 + P_0^2}$, the efficace current I_{so}, the voltage efficace V_{so}.

$$P_0 = R_s \cdot I_{so}^2 + \frac{\grave{V}^2}{R_F} \quad (11)$$
$$Q_o = \frac{\grave{V}^2}{L_s \cdot \omega} \quad (12)$$
$$\grave{V} = V_{so} \cdot \frac{R_F \cdot L_s \cdot \omega_s}{\sqrt{(R_s \cdot R_F)^2 + (L_s \cdot \omega_s \cdot (R_F + R_s))^2}} \quad (13)$$

The current I_{so} is very low in this test and the voltage losses due to the stator resistance are generally neglected before the voltage V_{so}, so from the previous equations we will have the following equations:

$$P_0 = \frac{V_{so}^2}{R_F} \quad (14)$$
$$Q_o = \frac{V_{so}^2}{L_s \cdot \omega_s} \quad (15)$$

Since the studied machine is a Squirrel-cage Class A (assumption of equal leakage distribution in the stator and rotor), therefore: $L_s = L_r$ [27-28].

During locked rotor and reduced voltage test (short circuit), the rotor is locked, so the speed is zero, which will imply that the slip is at its maximum value (g=1). The equivalent model of the machine is given in Figure 6.

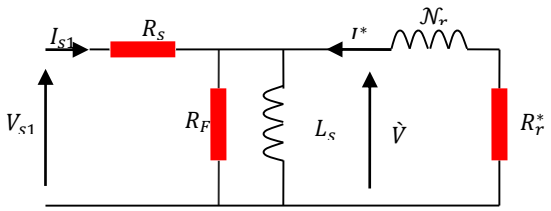

Fig. 6. Equivalent diagram of the locked rotor test machine

We have:

$$P_1 = R_s \cdot I_{s1}^2 + \grave{V}^2 \cdot \left(\frac{1}{R_F} + \frac{R_r^*}{(\mathcal{N}_r \cdot \omega_s)^2 + R_r^{*2}}\right) \quad (16)$$
$$Q_1 = \grave{V}^2 \cdot \left(\frac{1}{L_s \cdot \omega_s} + \frac{R_r^*}{(\mathcal{N}_r \cdot \omega_s)^2 + R_r^{*2}}\right) \quad (17)$$
$$\grave{V} = V_{s1} - R_s \cdot I_{s1} \quad (18)$$
$$\mathcal{N}_r = L_s \cdot \left(\frac{L_s^2}{M^2} - 1\right) \quad (19)$$
$$R_r^* = R_r \cdot \frac{L_s^2}{M^2} \quad (20)$$

As the voltage V_{s1} is low, it is possible to neglect the currents flowing in R_F and L_s before I_{s1} and the previous equations become :

$$P_1 = (R_s + R_r^*) \cdot I_{s1}^2 \quad (21)$$
$$Q_1 = \mathcal{N}_r \cdot \omega_s \cdot I_{s1}^2 \quad (22)$$

2.4. Electric Vehicle Model

The vehicle is subjected to forces along the longitudinal axis. There are types of three forces [1-2, 5]: -Rolling resistance force F_{tire} due to the friction of the vehicle tires on the road. It is given as:

$$F_{tire} = m \times g \times f_{ro} \quad (23)$$

With: m is the vehicle total mass, g is the gravity acceleration, fro is the rolling resistance force constant.
- Aerodynamic drag force F_{aero} caused by the friction on the body moving through the air. Its expression is:

$$F_{aero} = (1/2) \times \rho_{air} \times A_f \times C_d \times V^2 \quad (24)$$

With: ρ_{air} is the air density, A_f is the frontal surface area of the vehicle, C_d is the aerodynamic drag coefficient, V is the vehicle speed.

-Climbing force F_{slope} which depends on the road slope.

$$F_{slope} = m \times g \times sin(\beta) \quad (25)$$

With: β is the road slope angle.

The total resistive force F_r is given as:

$$F_r = F_{tire} + F_{aero} + F_{slope} \quad (26)$$

The load torque can be written as:

$$T_r = F_r \times \frac{r}{G} \quad (27)$$

where r is the tire radius, F_r is the total force.

By applying the fundamental principle of the vehicle dynamics, we can deduce the speed vehicle.

$$m\frac{dv}{dt} = F_t - F_r \quad (28)$$

where F_t is traction force. Table 3 summarizes the electric vehicle parameters.

Table 3. Parameters of the electric vehicle

Parameters	Symbol	Value	Unit
Vehicle total mass	m	1300	kg
Rolling resistance force constant	f_{ro}	0.01	
Air density	ρ_{air}	1.20	kg/m^3
Frontal surface area of the vehicle	A_f	2.6	m^2
Tire radius	r	0.25	m
Aerodynamic drag coefficient	C_d	0.32	
Gear speed ratio	G	5	
Road angle slope	β	60	°

3. DIRECT TORQUE CONTROL STRATEGY

To keep the DC bus voltage at a constant value when the speed of the rotor varies, different control techniques can be used. In our work, the IM is controlled using DTC strategy, which is a powerful control method for motor drives. The DTC technique is based on the independently control of the stator flux and electromagnetic torque.

For this purpose, the selection of the optimal space vector using a hysteresis controller is required. Similarly, the stator flux, electromagnetic torque developed by the machine and its position in terms of flux can be estimated [1-2].

Stator flux and electromagnetic torque are estimated using the following equations:

$$\begin{cases} \Phi_{s\alpha}(t) = \int_0^t (V_{s\alpha} - R_s * i_{s\alpha})dt \\ \Phi_{s\beta}(t) = \int_0^t (V_{s\beta} - R_s * i_{s\beta})dt \end{cases} \quad (29)$$

$$\Phi_s = \sqrt{\Phi_{s\alpha}^2 + \Phi_{s\beta}^2} \quad (30)$$

$$\theta_s = arctan\left(\frac{\Phi_{s\beta}}{\Phi_{s\alpha}}\right) \quad (31)$$

The electromagnetic torque is calculated using Equation 32.

$$\Gamma_e = \frac{3P}{2}\left(\Phi_{s\beta} i_{s\alpha} - \Phi_{s\alpha} i_{s\beta}\right) \quad (32)$$

The evolution of the stator flux in (αβ) frame is divided into six zones i, with i =[1: 6] as seen in Figure 7. The space vector applied in each condition is described in Table 4 [4-5].

Table 4. Switching table for the DTC technique

	N	1	2	3	4	5	6
H_Φ=1	H_Γ = 1	110	010	011	001	101	100
	H_Γ = 0	111	000	111	000	011	001
	H_Γ =-1	101	100	110	010	011	001
H_Φ=0	H_Γ = 1	010	010	011	001	101	100
	H_Γ = 0	000	000	111	000	111	000
	H_Γ =-1	001	001	101	100	110	010

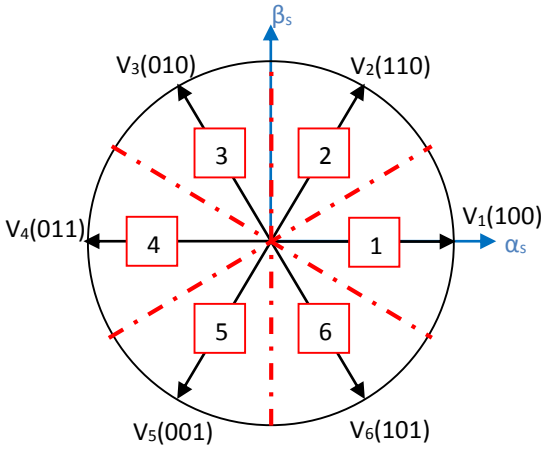

Fig. 7. The six voltage vector of the inverter

4. SIMULATION RESULTS AND DISCUSSION

MATLAB/Simulink has been used in the development of the DTC of induction motor using the above equations. The general studied system is represented in Figure 8.

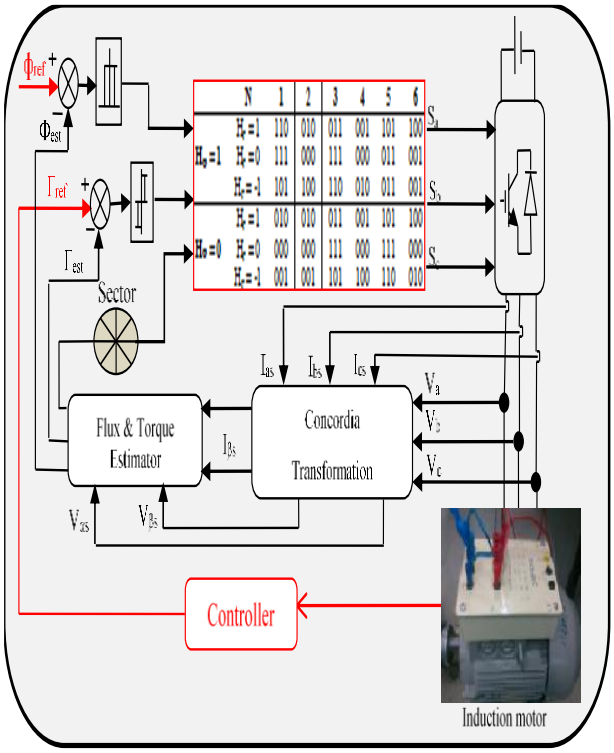

Fig. 8. General structure of the proposed direct torque control

The block diagram of the classical DTC is made under MATLAB/Simulink. The obtained results are given below. A vehicle speed profile is chosen to show the traction, the stop and the braking modes of the EV. The speed increases gradually from the moment t =9 s.

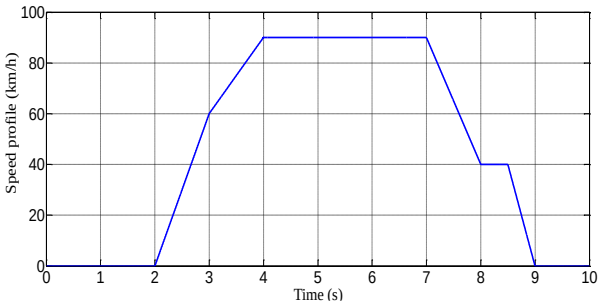

Fig. 9. Speed profile of the EV

The electromagnetic torque follows the load torque developed by the electric vehicle.

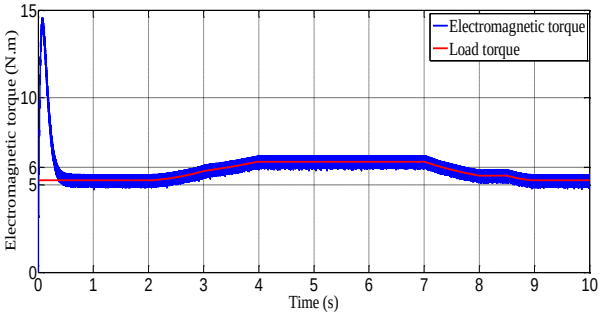

Fig. 10. Electromagnetic torque waveform

The biphase currents are in quadrature form (Figure 11) while the three-phase currents are shifted by $2\pi/3$ in Figure 12. The currents are alternative and reach a value of 5.6 A for a load torque of 6.3 N.m.

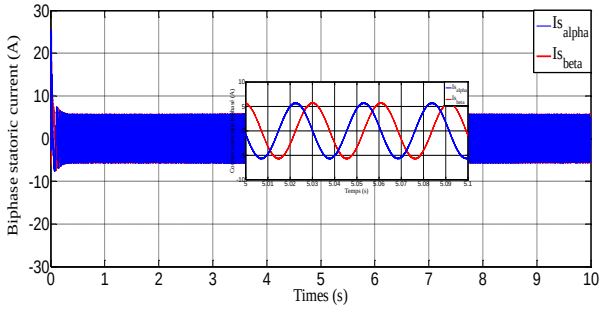

Fig.11. Biphase stator currents

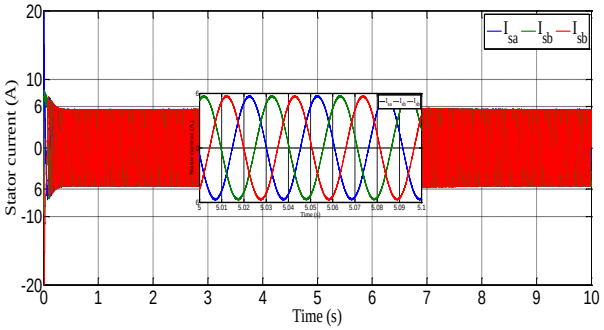

Fig. 12. Stator current waveform with classical DTC

The rotational speed of the induction is maintained to the reference imposed by the speed regulator (at 100 rad/s), despite the variation in the load applied to the electric machine. The direct and quadrature flux components are shifted by $\pi/2$ and have amplitude of 1Wb as shown in Figure 13. This amplitude is kept constant despite load torque variations.

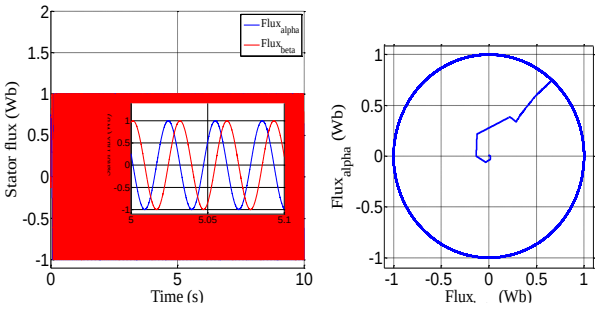

Fig. 13. Stator flux waveform and its circular trajectory

Although the DTC is insensitive to variations in the rotor parameters of the machine, the flow and torque estimation as well as the determination of the PI controller parameters are dependent on the stator resistance. This led us to the use of a controller ensuring total independence of the performances and accuracy of the technique with respect to the variation of the machine parameters.

6. CONCLUSION

An electric vehicle powered by the PEMFC is studied in this paper. The studied system deals the supply and the control of the electric vehicle using a sustainable energy and advanced control techniques. The obtained results show that the fuel cell insures the energy need of the EV. Firstly, a DTC method has been applied to control electric vehicle. Obtained results show the performances of the proposed system.

References

[1] F. Tazerart, Z. Mokrani, D. Rekioua, and T. Rekioua, Direct torque control implementation with losses minimization of induction motor for electric vehicle applications with high operating life of battery, Intern. Jour. of Hydrogen Energy, 39, 13827-38, (2015).

[2] Z. Mokrani, D. Rekioua, T. Rekioua, Modeling, Control and Power Management of Hybrid Photovoltaic Fuel Cells with Battery Bank Supplying Electric Vehicle, International Journal of Hydrogen Energy, 39(27), 15178-87, (2014).

[3] V. Oldenbroek, L. A Verhoef, and Ad. J. M. Van Wijk, Fuel cell electric vehicle as a power plant: Fully renewable integrated transport and energy system design and analysis for smart city areas, International Journal of Hydrogen Energy, 42(12), 8166-96, (2017).

[4] X. Lian, Wang, and J. Song, Fuel consumption optimization for smart hybrid electric vehicle during a car-following process, International Journal of Hydrogen Energy, 87, 17-29, (2017).

[5] D. Rekioua, E. Matagne, Optimization of photovoltaic power systems: Modelization, Simulation and Control, Green Energy and Technology, 102, (2012).

[6] N. Mebarki, T. Rekioua, Z. Mokrani, and D. Rekioua, Supervisor control for stand-alone photovoltaic/ hydrogen/ battery bank system to supply energy to an electric vehicle, International Journal of Hydrogen Energy, 39, 13777-88, (2015).

[7] S. G. Buja, Direct torque control of PWM inverter-Fed AC motor-a survey, IEEE Trans. Industrial Electronics, 4744-57, (2004).

[8] A. Haddoun, M. Benbouzid, D. Diallo, R. Abdessemed, J. Ghouili, and K. Srairi, A Loss-Minimization DTC Scheme for EV Induction Motor, IEEE Trans on Vehicular Technology, 56(1), 81-88, (2007).

[9] Z. Keliang, J.A. Ferreira , S.W.H. de Haan, Optimal energy management strategy and system sizing method for stand-alone photovoltaic-hydrogen systems, International Journal of Hydrogen Energy, 33(2), 477-489, (2008).

[10] D. Rekioua, S. Bensmail, N. Bettar, Study of hybrid photovoltaic/fuel cell system for stand-alone applications, International Journal of Hydrogen Energy, 39(3), 13820-26. (2014).

[11] Y. Liu , X. Wu, L. Huang, SVPWM method for performance improvement of direct torque control, Qinghua Daxue Xuebao/Journal of Tsinghua University, 44 (7), 869-872, (2004).

[12] N. Cui, C. Zhang, Z. Lu, K. Li, Fast torque response control of high efficiency drives in electric vehicles based on voltage space vector, Diangong Jishu Xuebao/Transactions of China Electrotechnical Society, 24(3) , 61-66, (2009).

[13] D. Rekioua, T. Rekioua, DSP-controlled direct torque control of induction machines based on modulated hysteresis control, Proceedings of the International Conference on Microelectronics, ICM, art. no. 5418603, 378-381, (2009).

[14] R. Abdelli, D. Rekioua, T. Rekioua, A. Tounzi. Improved direct torque control of an induction generator used in a wind conversion system connected to the grid; ISA Transactions, 52(4). 525-538, (2013).

[15] S. Jiangua, C. Quanshi. Research of Electric Vehicle IM Controller Based on Space Vector Modulation Direct Torque Control, Proceeding of the Eighth International Conference on Electric Machine and Systems ICEMS, vol. 2, 1617-20, (2005).

[16] R. Toufouti, S. Meziane, H. Benalla, Direct Torque Control for Induction Motor Using Fuzzy Logic, ACSE Journal, 6(2),19-26, (2006).

[17] H. Ehsan, A. K. Davood, DTC-SVM Scheme for Induction Motors Fed with a Three-level Inverter, World Academy of Science, Engineering and Technology, vol. 44, 168-172, (2008).

[18] S. M. Gadoue, D. Giaouris, J. W. Finch, Artificial Intelligence-Based Speed Control of DTC Induction Motor Drives- a Comparative Study, Electric Power System Research, 79, 210-19, (2009).

[19] J. Q. Yang, J. Huan, Direct Torque Control System for Induction Motors with Fuzzy Speed PI Regulator, IEEE Proceeding of the fourth International Conference on Machine Learning and Cybernetics, Guangzhou, vol. 2, 778-783, (2005).

[20] S. Gowrishankar, K. Kirshnamoorthi, Speed Control of Induction Motor Using PI and Fuzzy Controller, Journal of Innovative Research and Solution (JIRAS), 1A(2). 50-57, (2013).

[21] Y. Goa, J. Wang, X. Qiu, The Improvement of DTC System Performance on Fuzzy Control, 3rd International Conference on Environmental Science and Information Application Technology, vol. 10, 589-584, (2011).

[22] S. Tamalouzt, N. Benyahia, T. Rekioua, D. Rekioua, R. Abdessemed, Performances analysis of WT-DFIG with PV and fuel cell hybrid power sources system associated with hydrogen storage hybrid energy system, International Journal of Hydrogen Energy, 41(45), 21006-21, (2016).

[23] L. Yen-Shin, L. Juo-Chiun, New Hybrid Fuzzy Controller for Direct Torque Control Induction Motor Drives, IEEE Trans. Power Electronics , vol. 18, No. 5, 1211-19, (2003).

[24] S. Sharma, O. P. Jaga, and S. K. Maury, Modeling and Control Strategies for Energy Management System in Electric Vehicles, Perspectives in Science, vol. 8, 358-360, (2006).

[25] S. Taraft, D. Rekioua , D. Aouzellag , S. Bacha , A proposed strategy for power optimization of a wind energy conversion system connected to the grid Energy Conversion and Management, 101 , 489-502 (2015).

[26] F. Barrero, Gonzâlez, A. Torralba, E. Galvân, L. G Franquelo, Speed control of induction motor using fuzzy sliding-mode structure, IEEE Trans. Fuzzy Systems, 3375-83, (2004).

[27] J. J. Cathey, Electric Machines: Analysis and Design Applying Matlab, McGraw Hill, (2001).

[28] Z. Salleh, F. A. Patakor, A. N. A. Rashid, Study on parameter determination for 1.5kW AC induction motor, Conference: Seminar Penyelidikan Zon Utara 2013, At: Politeknik Tuanku Syed Sirajuddin, (2013).

Biographies

Zahra Mokrani received her master's degree in electrical engineering from the University of Bejaia, Algeria, in 2012. She is Ph.D. student in the same department since 2016. Her current research interests are electrical system and control.

E-mail address: mokrani-zahra@hotmail.fr

Djamila Rekioua obtained her engineering degree in electrical engineering in 1987, the master's degree, in 1993, both from National Polytechnic Institute of Algeria, and the Ph.D. degree in 2002. Her research interests include control of AC machines and electric drives, and renewable energies (photovoltaic, wind turbine, and hybrid systems). Since 1989, she is teaching and pursuing research; firstly at the University of Sciences and Technology, (Algeria) and now she is Professor at the University of Bejaia (Algeria), head of the Team Renewable Energy in LTII Laboratory of the University of Bejaia.

E-mail address: dja_rekioua@yahoo.fr

Toufik Rekioua received his engineering degree from the National Polytechnic Institute of Algeria and earned the Doctoral degree from I.N.P.L of Nancy (France) in 1991.
He is Professor at the Electrical Engineering Department-University of Bejaia (Algeria) since 1992. He is presently the director of the LTII laboratory. His research activities have been devoted to several topics: control of electrical drives, modelling, wind turbine and control in AC machines.

E-mail address: to_reki@yahoo.fr

Research Article | Submit Manuscript

Turkish Journal of Electromechanics & Energy

ISSN-2547-975X

Photovoltaic Parameters Estimation Using Hybrid Flower Pollination with Clonal Selection Algorithm

Ahmed K. Ryad[1, *], Ahmed M. Atallah[2], Abdelhaliem Zekry[3]

[1] Department of Electrical Power, International Academy for Engineering and Media Science, Giza, Egypt.
[2] Department of Electrical Power and Machines, Ain Shams University, Cairo, Egypt.
[3] Department of Electronics and Communications, Ain Shams University, Cairo, Egypt

Received: 6 November 2017; Revised: 16 August 2018; Accepted: 4 October 2018; Published: 1 December 2018
Turk J Electrom Energ Vol.: 3 No: 2 Page: 15-21 (2018)
SLOI: http://www.sloi.org/
*Correspondence E-mail: eng_ahmed_ryad@yahoo.com

ABSTRACT Extracting the parameters of photovoltaic (PV) cell is a vital process to accurately simulate the behavior of the cell. Various techniques are used to extract these parameters such as iterative, and metaheuristic methods. Although metaheuristic methods require more test points on the PV module, through this paper the optimization function is chosen to accurately adjust the I-V curve of the PV module based on less number of test points yet still achieve higher accuracy. A modified hybrid flower pollination method with clonal selection algorithm is suggested to extract the PV parameters and is compared with various metaheuristic methods to estimate the PV parameters of the single diode model, the two-diode model. In addition, modeling the PV at various irradiance and temperature levels was performed. Results show an excellent curve fitting for I-V characteristics and more accurate results in estimating the unknown parameters of PV cell.

Keywords: PV Model, Single Diode Model, Two Diode Model, Flower Pollination, Modified Flower Pollination

Cite this article: A. K. Ryad, A. M. Atallah, A. Zekry, Photvoltaic Parameters Estimation Using Hybrid Flower Pollination with Clonal Selection Algorithm, Turkish Journal of Electromechanics & Energy, 3(2), 15-21, (2018).

1. INTRODUCTION

The fast decline of conventional energy sources increases the need to use renewable energy sources. By 2016 renewable energies share by more than 24 % of total electricity consumption worldwide [1]. Energy generation based on photovoltaics is one of the most competitive renewable energy sources.

PV market is increasing rapidly and it is governed by the reduction in panel cost and increasing capacity factor. In 2016, PV contributed by at least 303 GW DC which is 4.8 GW more than the one from concentrated solar thermal power [1]. In Egypt, energies about 154 MW from photovoltaic cells and 3035 MW from solar panels were produced [2]. Various technologies are used to manufacture PV cells as crystalline silicon (monocrystalline, polycrystalline), thin film (amorphous silicon, Cadmium Telluride, copper indium gallium selenide), nanotechnology (tandem, super tandem, intermediate band) [3].

Modeling of PV cell is a fertile research area that aims to model the behavior of the cell using the electrical circuit to accurately predict the performance and efficiency. It helps to correctly track the maximum power point and simulate the whole system performance along with the power conditioning and storage units [4]. The model should be accurate, robust, take low computational time, gives correct I-V data close to experimental data at various working conditions [5].

Section (II) introduce the various model used to simulate PV characteristics, section (III) starts from Villalva et al. method to extract PV parameters while the current paper presents modification to eliminate the assumptions of Villalva method and produce an objective error function for extracting the required PV parameters based on five test points namely: maximum power, open circuit voltage, shorts circuit current, half open circuit voltage, average of maximum power voltage and open circuit voltage. The hybrid flower pollination with clonal selection algorithm (FPA-CSA) is suggested to minimize the objective error function. A lot of metaheuristic techniques was used in recent years to extract the PV parameters these techniques which varied in result accuracy, number of technique's parameters, technique complexity. Through this paper, a wide range of metaheuristic techniques was used to extract the PV parameters, and results showed that FPA-CSA provided

the least error when compared with famous metaheuristic techniques. FPA-CSA has more changeable parameters than the other techniques which increase the complexity of the algorithm. Section (IV) deals with extracting PV parameters at various environmental conditions mainly changing in irradiance and temperature using FPA-CSA technique.

2. THE PV MODEL

Various approaches are used to accurately simulate the behavior of PV cell, although circuit model of PV cell is the most popular approach which uses a relatively simple circuit model to simulate the electrical characteristics of PV cell [6, 33].

2.1. The Ideal Model of PV

As the PV cell is mainly a semi-conductor material, it can be modeled as the *P-N* junction that emits current when exposed to sunlight [6, 7].

The diode current is given as:

$$I_D = I_S * [\exp\left(\frac{q*V_D}{aKT}\right) - 1] \quad (1)$$

Where I_D is the diode current, I_s is the diode reverse saturation current, q is the absolute value of electron charge, V_D is the diode voltage, a is the diode ideality factor, K is the Boltzmann's constant and T is the cell temperature in Kelvin.

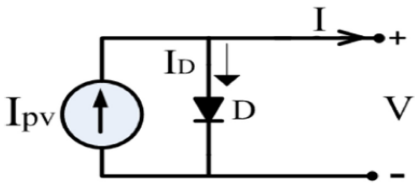

Fig.1. Ideal single diode model

The output current is given in Equation 2 where I_{pv} is the light current.

$$I = I_{PV} - I_S * [\exp\left(\frac{q*V_D}{aKT}\right) - 1] \quad (2)$$

Although the ideal model is simple, it can't provide a realistic model for PV behavior as it doesn't consider the effect of contact resistance between silicon and electrodes, electrode resistance and the leakage current.

2.2. Single Diode Model (with Rs and Rp).

The single diode circuit [8] is shown in Figure 2.

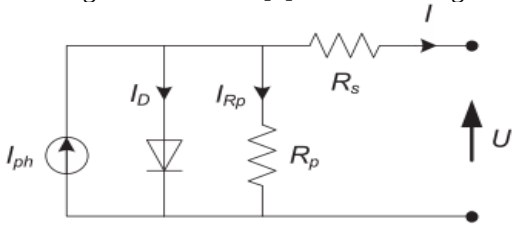

Fig.2. Single diode model

The output current is given in Equation 3 considering the effect of contact resistance by adding the series resistance (R_s) and the leakage current through adding shunt resistance (R_p).

$$I = I_{PV} - I_S\left[\exp\left(\frac{q*(V_D+I*R_S)}{aKT}\right) - 1\right] - \frac{V_D+I*R_S}{R_P} \quad (3)$$

2.3. Two-Diode Model

The two-diode model shown in Figure 3 compensates the effect of recombination current loss in the depletion region by adding a second diode to the PV cell model. The output current is given in Equation 4 where I_{S1} represents the first diode current and I_{S2} represents the recombination current. The advantage of this model is that unlike the single diode models, it provides appropriate accuracy in low irradiation values [6, 9-11].

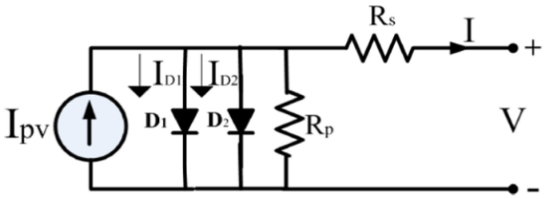

Fig.3. Two diode model

$$I = I_{PV} - I_{S1} * \left[\exp\left(\frac{q*(V_D+I*R_S)}{a_1 KT}\right) - 1\right] - \frac{V_D+I*R_S}{R_P} - I_{S2} * \left[\exp\left(\frac{q*(V_D+I*R_S)}{a_2 KT}\right) - 1\right] \quad (4)$$

According to Equation 4 the two-diode model takes into account the effect of the contact resistance and leakage resistance through adding the series resistance and the shunt resistance and the diode current through adding diode current I_{S1} and recombination current through adding second diode current I_{S2}.

2.4. Other PV Models

There is also three diode model, an explicit model that doesn't use equivalent circuit. It is used in a situation like resonance with cables, interaction with switching frequency harmonics, underdamped current. To model the reverse bias process and dynamic characteristics, a dynamic model is suggested [3, 12, 13].

3. ESTIMATING UNKNOWN PARAMETERS OF THE PV CELL

In general, the manufacturer datasheet provides special test points as the open circuit, short circuit and maximum power point voltage and current wherein single diode model there are five unknowns namely: photon current, saturation current, ideality factor, series resistance, and shunt resistance.

For the two-diode model, there are seven unknowns namely: photon current, series resistance, shunt resistance, first diode ideality factor, second diode ideality factor, first diode saturation current and second diode saturation current.

Finding the unknowns of the PV cell is essential to correctly simulate the cell behavior. Various methods are used to estimate these parameters as analytical methods, artificial intelligence and hybrid methods.

3.1. Villalva, Gazoli and Filho Model

Villalva et al. proposed a model to determine the five parameters of single diode model, based on adjusting I-V

curve to three common points: open circuit, short circuit, and maximum power point.

Three assumptions are used to find saturation current, ideality factor and light current as follow:

1. $1 \le a \le 1.5$
2. $I_{PV} \sim I_{SC.}$
3. $Io = \frac{I_{SC}+K_I*(T-To)}{\exp\left[\frac{(V_{OC}+K_V*[T-To])}{a*vt}\right]-1}$

where V_T is the thermal voltage and equals to ($N_s.k.t/q$) and N_s is the cells connected in series.

Two parameters are still unknown, namely series and shunt resistance. Those are adjusted based on a unique pair of (R_s, R_p) that match the maximum power point, in other words, the maximum power calculated by the model.

($P_{max,m}$) equal to datasheet maximum power ($P_{max,e}$), is given by the following equation [7, 14]:

$$P_{max,e}=V_{mp}[I_{pv} - Io(\exp(\frac{q}{kT}\frac{V_{mp}+R_sI_{mp}}{aN_s}) - 1) - \frac{V_{mp}+R_sI_{mp}}{R_P}] \quad (5)$$

3.2. Metaheuristics Methods

Metaheuristics methods can be used as an optimization technique for Equation 5, without assuming any parameter of the PV model [32].

Through this study, a range of metaheuristics methods are reviewed and used to optimize Equation 5, such as: Particle Swarm (PS)[15,16], Genetic Algorithm (GA)[17], Pattern Search (Pt.S)[18], Simulated Annealing (SA)[19], Cuckoo Search [20, 21, 22] (CS) and Hybrid Cuckoo Search with Nelder-Mead Simplex(CS-NMS)[23], Whale Optimization Algorithm (WOA)[24-25], Grey Wolf Algorithm (GWA)[26], Ant Lion Algorithm (ALA) [27], Flower Pollination Algorithm (FPA) [28], Hybrid Flower Pollination with Clonal Selection Algorithm (FPA-CSA) [29].

FPA-CSA is considered to minimize the objective function to extract PV parameters, where flower pollination algorithm is enhanced by combining it with the clonal operator in current study.

Flower pollination is the process of transferring pollen between flowers through pollinator, and this process can be cross-pollination or self-pollination. In cross-pollination, pollens from different plants can be transferred while in self-pollination only pollens from same plant type are transferred. This process can also be biotic which needs a pollinator or abiotic which needs no pollinator. Another important property is the plant constancy property where plant attract the pollinators to it and by-pass other plants. The pollination process can be either local (abiotic and self-pollination) or global (biotic and cross-pollination), so a switch probability *P* is presented to switch between the two types of pollination.

The clonal selection algorithm is based on generating antibodies for various viruses each of them is activated by a certain virus and the selected antibodies are cloned and mutated.

The principle of hybridization is presented in [29], where local pollination step size is scaled, then the best solutions are selected at each population. The best 14 solutions were selected and cloned proportionally to its fitness as the pseudo code of the algorithm in this study as it is shown in Table 1.

The reason why FPA-CSA provide more accurate results lays on having the property of global pollination from FPA algorithm which clonal selection enhance by choosing the best solution and cloning them.

Table 1. Pseudo-Code of FPA-CSA

1- Minimize or maximize the objective function **f(x)**, x=(x1, x2,….xd)
2- Create a random initial population **pop** of the size n.
3- Identify **g*** which is the best solution in **pop.**
4- Identify **P ε [0,1]** which is a switch probability between global and local pollination.
5- **While** (gen < Max Generation Num)
6- **If rand > p**, // perform global pollination
7- For each Xi in the Pop
8- Draw a (d-dimension) step vector L which obeys a levy distribution.
9- Global pollination via $X_i^{t+1} = X_i^t + \gamma_1 L(g^* - X_i^t)$
10- **End for**
11-**Else**
12- Select best m solutions from the **Pop** to form **ClonesPop** population.
13- Clone solution in **ClonesPop** proportional to affinity.
14- **For** each solution in **ClonesPop**
15- Draw ε from a uniform distribution in [0,1].'
16- Randomly choose j and k from **Pop.**
17- Perform local pollination via $\mathbf{X_i^{t+1} = X_i^t + \gamma_2\varepsilon (X_j^t - X_k^t)}$.
18- **End for**
19- **End if.**
20- Select best solutions from **Pop** and **ClonesPop** to from **NewPop** population.
21- Replace **Pop** by **NewPop.**
22- Find the current best solution **g***.
23- If **g*** doesn't chane, for the successive 100 iteration, with a value more than 10^{-6}, keep **g*** .
24- Replace **Pop** by a new randomly generated one.
25- gen=gen+1.
26- **End while.**
27- **Print g***

The previous algorithms are tested using MATLAB software, and with a computer equipped with an Intel Core i5 processor. A list of parameters used for each algorithm is shown in the Table 2 (2,000 iterations for each), under same bounds.

Table 2. Parameters of metaheuristic methods

Algorithm	*Parameters*
Particle Swarm	35 Particles
Cuckoo Search	35 Nests, discovery rate = 0.25.
ALA	35 Search Agent
WOA	35 Search Agents
FPA	Population size 35, Probability switch: 0.8 γ = 0.01, for Levy flight λ = 1.5
GWA	35 Search Agents
FPA-CSA	Population size: 35, Probability switch: 0.8, cloning array = [9, 8, 7, 6, 5, 4, 3, 2, 1, 1, 1, 1, 1, 1], γ 1 = 1, γ2 = 3, for Levy flight λ = 1. 5

For PS, GA, PS and SA, default built-in MATLAB codes were used in the test.

Each method is used to estimate the five unknown parameters of single diode model based on single optimization function by minimizing the absolute error of ($P_{max,m}$-$P_{max,e}$) proposed by Villalva et al in Equation 5. For both Astro power AP 110 model and Kyocera KC-40T shown in Appendix I & II. SA, then FPA-CSA provide superior error as shown in Table 3, which makes

the maximum power point matches exactly with one reported in the datasheet point I-V curve for SA method was plotted in Figure 4 to clearly identify the models fitting with the rest of remarkable points mainly open circuit and short circuit.

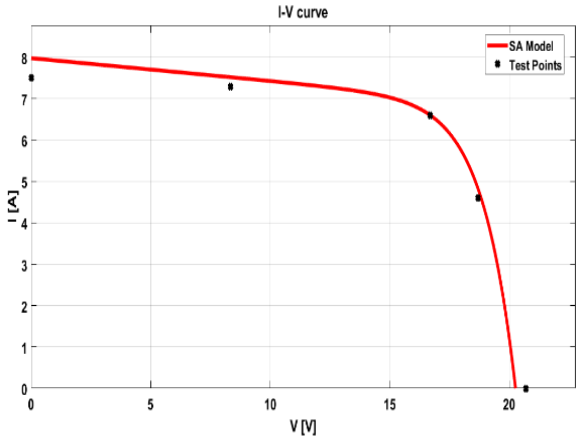

Fig. 4. I-V curve using SA algorithm based on Villalva et al. for single diode model for AP-110 Module

Although SA presents extremely small error in calculating the maximum power point but it doesn't fit curve in other points as in open circuit and short circuit points as the objective function only accounts on maximum power point and no assumption is made for other unknowns.

On the other hand, the objective function can be based on the summation of error as shown in [30], so the objective function can be modified to consider five test points namely: open circuit, short circuit, maximum power point, half open circuit voltage and average of maximum power voltage and open circuit voltage as follows:

$$\text{Error}=\text{Abs}\,(P_{max,m}-P_{max,e})+\text{Abs}\,(V_{oc,m}-V_{oc,e})+\text{Abs}\,(I_{sc})+\text{Abs}\,(V_{x,m}-V_{x,e})+\text{Abs}\,(V_{xx,m}-V_{xx,e}) \quad (6)$$

where V_x is half of the voltage at maximum power point and V_{xx} is average of maximum power voltage and open circuit voltage test point based on M. Siddiqui et al. [30].

To determine the efficiency each metaheuristic method is tested to find the least error when applied to suggested error optimization function, a summary of results is found in the Table 4.

FPA-CSA then CS provide better results than the other methods, I-V curve is plotted to examine fitting the data in Figure 5.

Where I_O= 1.5246e-06 A, I_{PV}= 7.5135 A, a= 1.4576, R_P=49.9999Ω, R_S= 0.08999Ω.

Table 4. Results of metaheuristic methods for AP 110 Model based on five test points for single diode model.

Algorithm	*Error*
Genetic Algorithm	0.4041
Particle Swarm	0.542
Pattern Search	1.159
Simulated Annealing	1.095
Cuckoo Search	0.3768
Cuckoo Search- Nelder-Mead	0.5733
Ant Lion	0.6420
Whale Algorithm	0.4284
Flower Pollination	0.3816
Grey Wolf Optimizer	0.5118
Flower Pollination- Clonal Selection	**0.373**

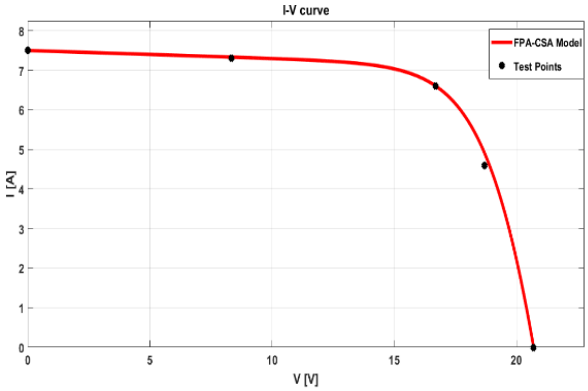

Fig. 5. I-V Curve for AP-110 module using FPA-CSA using single diode model based on five test points

The model present very good fitting for I-V characteristics with a slight error.

Again, the metaheuristic methods were tested to extract the parameters of two diode model for AP-110 module based on the previous five test points as shown in the Table 5.

Table 5. Two-diode model optimization results for metaheuristic methods

Algorithm	*Error*
Genetic Algorithm	0.5166
Particle Swarm	0.4076
Pattern Search	0.7476
Simulated Annealing	0.7529
Cuckoo Search	0.3964
Cuckoo Search- Nelder-Mead	0.6035
Ant Lion	0.56634
Whale Algorithm	1.2788
Flower Pollination	0.4073
Grey Wolf Optimizer	0.83851
Flower Pollination- Clonal Selection	**0.3739**

Table 3. Results of meta-heuristic methods and estimated five parameters

	GA	*PS*	*Pt. S*	*SA*	*CS*	*CS-NMS*	*ALA*	*WAO*	*FPA*	*GWA*	*FPA-CSA*
Error	5.4e-6	4.3e-7	8.4e-08	5.6e-14	2.5e-6	1.9e-7	1.9e-9	1.2e-8	5.9e-6	2.01e-5	1.4e-9
Io	1.95e-6	1.50e-6	1.00e-6	3.20e-6	4.98e-6	1.24e-6	4.99e-6	1.06e-6	1e-6	1.85e-6	2.8e-6
Ipv	7.80	7.65	7.12	7.84	7.91	7.99	8	7.86	7.42	8	7.50
A	1.41	1.42	1.50	1.45	1.49	1.43	1.50	1.46	1.43	1.48	1.49
Rp	38.25	36.03	48.19	40.45	49.53	16.25	49.99	18.35	38.73	16.75	42.21
Rs	0.020	0.038	0.010	0.010	0.030	0.011	0.048	0.072	0.057	0.016	0.012

Once again FPA-CSA then CS present more accurate results in the two-diode model to accurately detect the seven model parameters based on minimizing the error in Equation 6.

The seven parameters extracted using FPA-CSA are as shown in Table 6.

Table 6. Seven parameters extracted using FPA-CSA for AP 110 model

Parameter	*Value*
I_{01}	1.743159e-08 A
I_{PV}	1.743159e-08 A
a_1	1.4579
R_P	50 Ω
R_S	0.090 Ω
I_{O2}	1.5072e-06 A
a_2	1.4576

I-V curve of the seven-parameter model using FPA-CSA is shown in Figure 6.

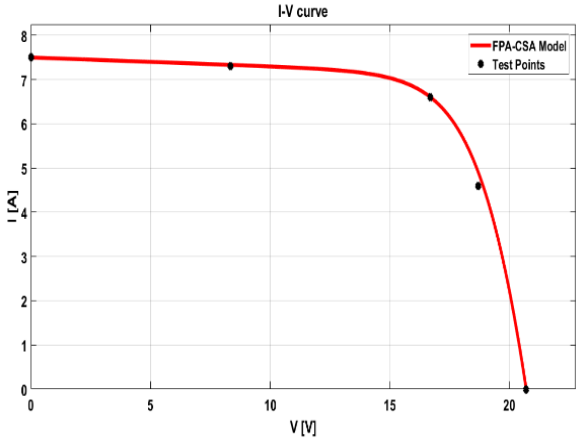

Fig.6. I-V curve of the seven-parameter model using FPA-CSA two diode model based on five test points

For convenience, the best two metaheuristic methods namely: FPA-CSA and CS were tested to extract two diode parameters for KC-40T model where errors were computed as 0.0358 and 0.0426, respectively. It was shown again that FPA-CSA shows superiority over other methods.

Two diode model parameters for KC-40T are shown in Table 7.

Table 7. Seven parameters extracted using FPA-CSA for AP 110 model

Parameter	*Value*
I_{O1}	2.4299e-08 A
I_{PV}	2.6486A
a_1	1.69999
R_P	2.13128e3 Ω
R_S	0.45439 Ω
I_{O2}	1.146e-08 A
a_2	1.219

4. MODELING OF PV CELL AT DIFFERENT IRRADIANCE LEVEL AND TEMPERATURES

The previous work models the PV cell at reference conditions namely 1000 W/m^2 irradiance at 25 °C.

It is necessary to model the PV cell at various environmental conditions, mainly the irradiance level and temperature, as the unknown parameters of the PV depend on both irradiance and temperature [31, 34].

The MPF-CSA is tested to estimate the parameters of two diode model for the KC-40T model at low irradiance, namely 400 W/m^2 and at 50 °C, based on test points in [30]. Results are shown in Figure 7 which show excellent fitting for the I-V characteristics at various operating conditions.

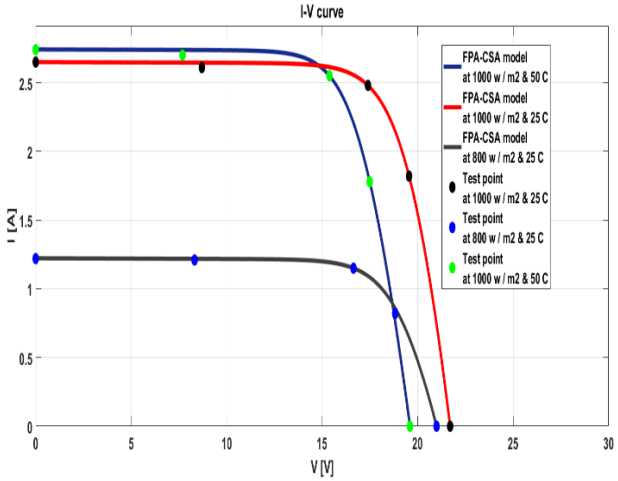

Fig. 7. Two diode model at 1000 W/m^2 + 25°C, 400 W/m^2 + 25°C and 1000 W/m^2 + 50°C for KC-40T model

4. CONCLUSION

Flower pollination algorithm hybridized along with colonel selection algorithm (FPA-CSA) was tested to extract the parameters of PV module along with various metaheuristic methods. Firstly, objective function depends only on settling the I-V curve on MPPT, SA then FPA-CSA where the most effective methods with the least errors 5.68e-14, 1.40e-9 respectively. Although these results are rather tricky as settling the curve at only MPPT doesn't ensure fitting the entire curve.

A proposed modification on the objective function was introduced in order to fit the curve at common point as open circuit voltage, short circuit current, half open circuit voltage, average of maximum power voltage and open circuit voltage along with MPPT. Results in Tables 3, 4 shows the FPA-CSA ranks as number one among other metaheuristic methods followed by FPA and CS methods as shown in Figure 8.

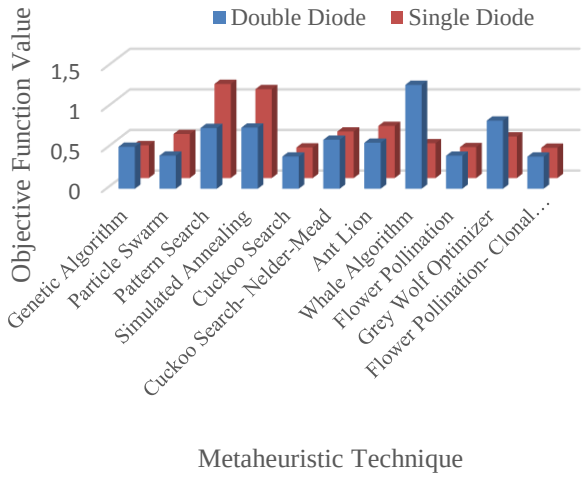

Fig. 8. Comparison between metaheuristic methods objective function result for both single diode model and double diode model

The obtained I-V curve based on the suggested objective function using FPA-CSA produce the most accurate curve fitting to the practical test points with the least error.

Either five parameters model or seven parameters model proved to provide high accuracy and less error in modeling even when compared with a variety of artificial intelligence techniques such as particle swarm, genetic algorithm, simulated annealing, etc.

Objective function better includes minimization of error in the five remarkable points (OC, SC, MP, V_x, and V_{xx}) for more accurate results which require only two test points as first three points are typical datasheet information.

Further addition of experimental points can improve the accuracy of the model although it increases the complexity of the objective function.

Although FPA-CSA has more parameters which make it more complex compared to original FPA it provides more accuracy, the problem of excessive parameters can be handled as a separate optimization problem to select the appropriate parameters for the required problem.

The proposed algorithm works efficiently with various environmental conditions and presents accurate modeling for the PV cell especially with two diode model. It presents more accurate results at low irradiance level.

Further improvement can be made by having a secondary optimization problem which include estimation of sensitivity parameters of the transitional equations to exclude the need for various test points at different environmental conditions [34].

The modeled PV circuit can be used to simulate the PV behavior at actual environment along with normal and faulty conditions thus predicting cell behavior and providing appropriate precautions.

References

[1] REN21 (2018), Renewables 2018 Global Status Report (Paris: REN21 Secretariat). ISBN 978-3-9818911-3-3, http://www.ren21.net/status-of-renewables/global-status-report/ (Accessed 30.06.2018).

[2] IRENA (2017), Renewable Energy Statistics 2017, The International Renewable Energy Agency, Abu Dhabi, https://www.irena.org/publications/2017/Jul/Renewable-Energy-Statistics-2017 (Accessed 30.06.2018).

[3] M. E. Şahin, H. İ. Okumuş, Physical Structure, Electrical Design, Mathematical Modeling and Simulation of Solar Cells and Modules, Turkish Journal of Electromechanics & Energy, 1(1), (2016).

[4] V. J. Chin, Z. Salam, and K. Ishaque, Cell Modeling and model parameters estimation techniques for photovoltaic simulator application: A review, Appl. Energy, vol. 154, 500–519, (2015).

[5] N. Barth, R. Jovanovic, S. Ahzi, and M. A. Khaleel, PV panel single and double diode models: Optimization of the parameters and temperature dependence, Solar Energy Materials and Solar Cells, vol. 148, 87–98, (2016).

[6] A. R. Jordehi, Parameter estimation of solar photovoltaic (PV) cells: A review, Renew. Sustain. Energy Rev., vol. 61, pp. 354–371, (2016).

[7] M. Villalva, J. Gazoli, and E. Filho, Comprehensive Approach to Modeling and Simulation of Photovoltaic Arrays, IEEE Trans. Power Electronics, 24(5),1198–1208, (2009).

[8] M. S. Ebrahim, A.M. Sharaf, A. M. Atallah, A. S. Emareh, An Efficient Controller for Standalone Hybrid- PV Powered System, Turkish Journal of Electromechanics & Energy, 2(1), (2017).

[9] J. Gow, C. Manning, Development of a model for photovoltaic arrays suitable for use in simulation studies of solar energy conversion systems, Sixth International Conference on Power Electronics and Variable Speed Drives, Conf. Publ. No. 429, 69-74 (1996).

[10] S. Chowdhury, G. A. Taylor, S. P. Chowdhury, A. K. Saha, Y. H. Song, Modeling, simulation and performance analysis of a PV array in an embedded environment, 42nd International Universities Power Engineering Conference, vol.42,781-785, (2007).

[11] S. Gupta, H. Tiwari, M. Fozdar, V. Chandna, Development of a two-diode model for photovoltaic modules suitable for use in simulation studies,2012 Asia-Pacific Power and Energy Engineering Conference, 1-4, (2012).

[12] K. Nishioka, N. Sakitani, Y. Uraoka, T. Fuyuki, Analysis of multi-crystalline silicon solar cells by modified 3-diode equivalent circuit model taking leakage current through periphery into consideration, Solar Energy Materials and Solar Cells, 91(13),1222–7, (2007).

[13] K.A. Kim, C. Xu, L. Jin, P.T. Krein, A dynamic photovoltaic model incorporating capacitive and reverse-bias characteristics, IEEE Journal of Photovoltaics, 3(4), 1334–41, (2013).

[14] G. Ciulla, V. Lo Brano, V. Di Dio, and G. Cipriani, A comparison of different one-diode models for the representation of I-V characteristic of a PV cell, Renew. Sustain. Energy Rev., vol. 32, 684–696, (2014)

[15] M. Ye, X. Wang, Y. Xu, Parameter extraction of solar cells using particle swarm optimization, Journal of Applied Physics, vol.105, 1-8, (2009).

[16] S. Jing Jun, L. Kay-Soon, Photovoltaic model identification using particle swarm optimization with inverse barrier constraint, IEEE Trans Power Electronics, 27(9), 3975–83, (2012).

[17] M. S. Ismail, M. Moghavvemi, TMI Mahlia, Characterization of PV panel and global optimization of its model parameters using genetic algorithm, Energy Convers Manage, vol.73, 10–25, (2013).

[18] M. F. AlHajri, K. M. El-Naggar, M. R. AlRashidi and A. K. Al-Othman, Optimal extraction of solar cell parameters using pattern search, Renewable Energy, vol. 44, 238-245, (2012).

[19] K. M. El-Naggar, M. R. AlRashidi, M. F. AlHajri and A. K. Al-Othman, Simulated annealing algorithm for photovoltaic parameters identification, Solar Energy, vol.86, 266–74, (2012)

[20] X. Yang, Nature-Inspired Metaheuristic Algorithms Nature-Inspired Metaheuristic Algorithms, Second Edition, (2010).
[21] J. Ma, T. O. Ting, K. L. Man, N. Zhang, S. U. Guan, and P. W. H. Wong, Parameter estimation of photovoltaic models via cuckoo search, Journal of. Applied. Mathematics., vol. 2013, 10–12, (2013).
[22] X.-S. Yang, and S. Deb, Engineering Optimization by Cuckoo Search, Int. J. Mathematical Modelling and Numerical Optimization, vol.1, 1–17, (2010).
[23] R. Jovanovic, S. Kais, and F. H. Alharbi, Cuckoo Search Inspired Hybridization of the Nelder- Mead Simplex Algorithm Applied to Optimization of Photovoltaic Cells, Appl. Math. Inf. Sci, 10(3), 961–973, (2016).
[24] S. Mirjalili and A. Lewis, The Whale Optimization Algorithm, Adv. Eng. Software, vol. 95, 51–67, (2016).
[25] D. Oliva, M. Abd El Aziz, and A. Ella Hassanien, Parameter estimation of photovoltaic cells using an improved chaotic whale optimization algorithm, Appl. Energy, vol. 200, 141–154, (2017).
[26] S. Mirjalili, S. M. Mirjalili, and A. Lewis, Grey Wolf Optimizer, Adv. Eng. Software, vol. 69, 46–61, (2014).
[27] S. Mirjalili, The ant lion optimizer, Adv. Eng. Software, vol. 83, 80–98, (2015).
[28] D. F. Alam, D. A. Yousri, and M. B. Eteiba, Flower Pollination Algorithm based solar PV parameter estimation, Energy Conversion and Management, vol. 101, 410–422, (2015).
[29] E. Nabil, A Modified Flower Pollination Algorithm for Global Optimization, Expert Systems with Applications, vol. 57, 192–203, (2016).
[30] M. U. Siddiqui, a. F. M. Arif, a. M. Bilton, S. Dubowsky, and M. Elshafei, An improved electric circuit model for photovoltaic modules based on sensitivity analysis, Solar. Energy, vol. 90, 29–42, (2013).
[31] M. A. Abido and M. S. Khalid, Seven-parameter PV model estimation using Differential Evolution, Electrical Engineering, 100(2), 971-981, (2018).
[32] D. S. Pillai and N. Rajasekar, Metaheuristic algorithms for PV parameter identification: A comprehensive review with an application to threshold setting for fault detection in PV systems, Renew. Sustain. Energy Rev., 82(3), 3503–3525, (2018).
[33] M. U. Siddiqui and M. Abido, Parameter estimation for five- and seven-parameter photovoltaic electrical models using evolutionary algorithms, Applied Soft Computing. J., 13(12), 4608–4621, (2013).
[34] H. Ibrahim and N. Anani, Variations of PV module parameters with irradiance and temperature, Energy Procedia, vol. 134, 276–285, (2017).

APPENDICES

Appendix I: Data of KC 40 T Model at 1000 W/m^2 and 25 °C

Parameter	Value
I_{SC}	2.65
V_{OC}	21.7
I_{MP}	2.48
V_{MP}	17.4
N_S	36
Current Temp. Coefficient	0.00106
Voltage Temp. Coefficient	-0.0821

Appendix II: Data of AP 110 Model at 1000 W/m^2 and 25 °C

Parameter	Value
I_{SC}	7.5
V_{OC}	20.7
I_{MP}	6.6
V_{MP}	16.7
N_S	36
Current Temp. Coefficient	0.0034
Voltage Temp. Coefficient	-0.08

Biographies

Ahmed Kamal Ryad is an assistant lecturer at the department of electrical power in International Academy for Engineering and Media Science, Egypt. He, received his B.Sc and M.Sc degrees from Electrical Power and Machine Department, Ain Shams University, Cairo, Egypt, in 2010 and 2014 respectively. He is currently working to finalize his Ph.D. His current research includes photovoltaic cells and artificial intelligence.
E-mail: eng_ahmed_ryad@yahoo.com

Prof. Ahmed Mohamed Atallah earned his B.Sc. and M.Sc. degrees from Electrical Power and Machine Department, Ain Shams University, Cairo, Egypt, in 1979 and 1984, respectively. He was awarded with Ph.D. from Department of Electrical Engineering, University of Alberta, Edmonton, Canada, in 1988. His research interest includes renewable energies.
E-mail: ahmed_atallah@eng.asu.edu.eg

Prof. Abdelhaliem Zekry is a professor of electronics at the faculty of engineering, Ain Shams University, Cairo, Egypt. He worked at several universities. He published more than 140 journal and conference papers. He also supervised more than 60 Master thesis and 23 Doctorate theses in the areas of electronics and electronics for communications as well as in photovoltaics. Prof. Zekry's research focuses on the fields of microelectronics and electronic applications including communications and photovoltaics.
E-mail: a3zekrey@gmail.com

Research Article | Submit Manuscript

Turkish Journal of Electromechanics & Energy

ISSN-2547-975X

Estimation of Voltage Profile and Short-Circuit Currents for a Real Substation Distribution System

Alkan Aksoy[1*], Fatih Mehmet Nuroğlu[2]

[1]Karadeniz Technical University, Abdullah Kanca Vocational School, Sürmene, Trabzon, Turkey
[2]Karadeniz Technical University, Department of Electrical and Electronics Engineering, Trabzon, Turkey

Received: 13 August 2018; Revised: 28 October 2018; Accepted: 6 November 2018; Published: 1 December 2018
Turk J Electrom Energ Vol.: 3 No: 2 Page: 22-27 (2018)
SLOI: http://www.sloi.org/
*Correspondence E-mail: alkanaksoy@ktu.edu.tr

ABSTRACT Electrical energy demands gradually increasing in the world in each year, and numerous power plants continue to be installed to supply required energy. Most of these are small-scale power plants established at different terrains. The power produced by the power plants is transmitted to the existing transmission and distribution lines in the Black Sea region of Turkey. So, the electrical network is becoming increasingly complex. Distributed generations affect the electrical system in many ways. The goal of this study is to determine the effects of distributed generation on Trabzon city's Araklı-II feeder such as voltage profile and short-circuit currents of bus bars. The system modeled and simulated by using the DIgSILENT Power Factory software with real parameters. It was found that distributed generation sources have positively affected the voltage level of bus bars yet highly single-phase and three-phase short-circuit currents was observed.

Keywords: Load Flow, Short Circuit Analysis, Distributed Generation, Radial Distribution System

Cite this article: A. Aksoy, F. M. Nuroğlu, Estimation of Voltage Profile and Short-Circuit Currents for a Real Substation Distribution System, Turkish Journal of Electromechanics & Energy 3(2) 22-27 (2018).

1. INTRODUCTION

Both demand and supply of electricity is continuously increasing in the world due to population growth and industrial development [1]. As a result, several distributed generators (DGs) have been are built to be used in electric power plants recent years in Turkey [2]. These power plants are usually located close to the energy source and the existing distribution network [3]. DGs are connected to radial network and change the voltage profile and short circuit current [4]. The electrical devices work efficiently if the voltage profile and stability is in the range of nominal values. In addition, relay protection and coordination are very important for power stability [5].Coordination of electrical systems mostly depends on the voltage level and short-circuit currents value. Nowadays, these parameters are calculated using by software instead of conventional methods [6]. Arsin substation center contains industrial feeder, household feeders and two DGs which are connected to the different points of busbar. This connecting situation of DGs on busbar is the reason for choosing this substation as study of interest. This study aims to report the changes in voltage profile, single phase-ground and three phase short- circuit currents on busbar and terminals according to electric generation parameters of DGs.

2. ANALYSES OF FEEDERS

Single line diagram of the Arsin substation is shown in Figure 1. Arsin substation has two power transformers (TR). TR-A's is 25 MVA power transformers while TR-B's power is 50 MVA. When higher electrical power is demanded from substation, both of two transformers are activated, otherwise only TR-B is activated. The vector group of these transformers designed as YNyn0. The neutral point of the primer side of power transformers grounded directly and neutral point of secondary side is grounded over 20 ohm resistance, separately. Line diagram of Araklı-II feeder is shown in Figure 2. DG-I and DG-II are 14 km and 19 km away from the transformer center, respectively.

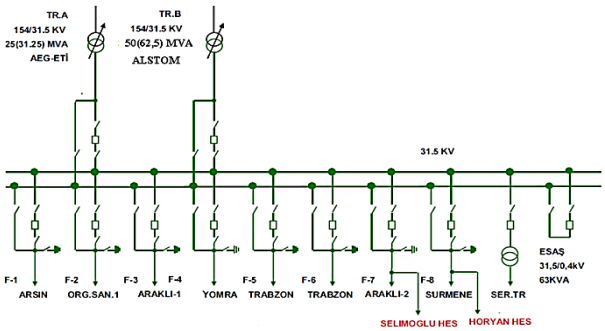

Fig. 1. Single-line diagram of Arsin substation [7]

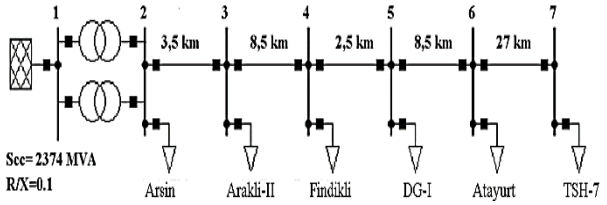

Fig. 2. Single-line diagram of Araklı-II feeder

The substation center and all feeders which were modeled using DIgSILENT Power Factory software are seen in Figure 3. This established model was based on data provided from Çoruh Electricity Distribution Company (Çoruh EDAS Corp.) and which is one of the 14 district offices of Turkey Electricity Transmission Company (TEIAS). The network model was examined with four cases according to the situation of DGs. These cases are, both DGs deactivated (Case-I), only DG-I activated (Case-II), only DG-II activated (Case-III), and both DGs activated (Case-IV). The delivery power which is used for load flow analysis are selected as the lowest and highest powers recorded on distribution grid system in January 2015. Also, load flow estimation analyses were performed for the years of 2020 and 2025. In addition, short-circuit current for single-phase to ground and three-phase were calculated in selected bus bar.

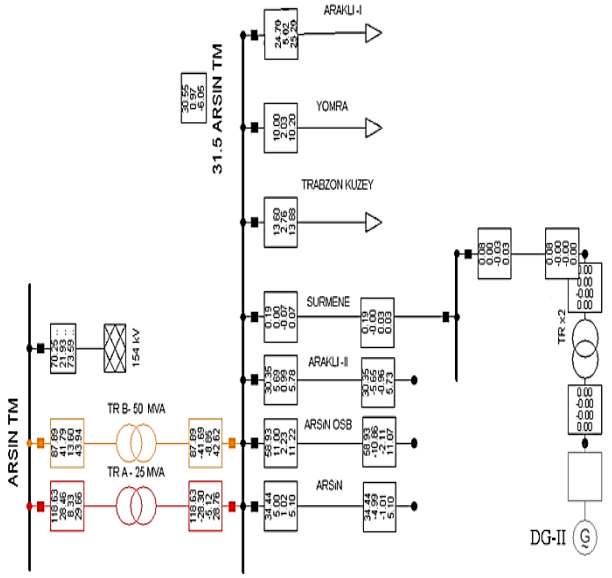

Fig. 3. Çoruh EDAS Corp. Arsin substation loading estimation model for year 2025 without DGs

Short relative circuit voltage value (U_k %) of TR-A and TR-B are reported as 9.1 % and 12.3 % respectively. Maximum three-phase short-circuit current value of Arsin substation center is 8.9 kA and short-circuit cutting power value is 2374 MVA [7]. Two different DGs are connected to substation from two different points of feeders. Each power plant has two generator units which are running in parallel mode. The characteristics of these generators are given in Table 1. Generator stator windings are grouped in star type. Output voltage values of stator windings for DG-I and DG-II are 6.3 kV. On the other hand, neutral resistance values of stator windings are 365 ohm and 364 ohm respectively. Vector groups of voltage step-up transformers is Dyn11 (delta-grounded wyes) type and their nominal powers are 5.5 MVA, 3.375 MVA, respectively. The relative short circuit voltage U_k % value of these transformers is 7% and neutral resistance values are 20 ohm.

Table 1. Technical information of DG

DG-I	Xd	1.409	Xq	1.394
	X'd	0.259	X'q	1.394
	X"d	0.186	X"q	0.237
	P(MW)	4.5	Cosφ	0.90
DG-II	Xd	1.123	Xq	0.620
	X'd	0.211	X'q	0.620
	X"d	0.157	X"q	0.185
	P(MW)	3	Cosφ	0.85

The length of the Araklı -II line is 50 km long and radial type. DG-I is connected to this line. On the other hand, DG-II is connected to the substation with a separate 477 MCM line. Araklı-II feeder has 99 distribution transformers. Total nominal power for each of these transformers is about 10 MVA as shown in Table 2. These transformers have a different connection groups according to their rated power. Yzn11 connection group which have a nominal power value of 160kVA and below is used in transformers while Dyn11 connection group is used in transformers which have a nominal power value above 160 kVA.

Table 2. Technical information and quantity of transformer on Arakli-II feeder

Power (kVA)	50	100	160	250	400
Quantity	37	49	7	3	3
U_k %	4.5	4.5	4.5	4.5	4.5

2.1. Voltage Profile

DG can change the feeder voltages, and voltage drop is caused by the line impedance and current. The allowable voltage limits are defined in regulation [8]. According to IEC 1547 standards DGs are not expected to support the voltage control, actively. Nevertheless, voltage of the feeder can be changed by the DG type and operation region (grid sub excited or overexcited) [9]. Many values such as network power losses, amplitude of the busbar voltage, angle and power values are calculated using basic variables such as; Q: Reactive Power, P: Active Power, V: Busbar Voltage and δ: Phase Angle.

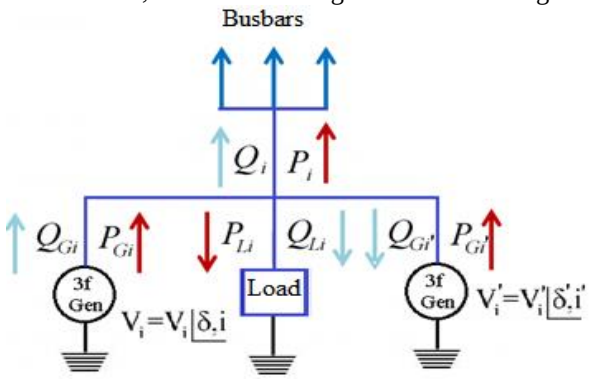

Fig. 4. Representation of basic load flow

Basic load flow scheme is shown in Figure 4. The generator transmits active power to the grid. However, the reactive power exchange is bidirectional. Particularly distributed generation sources use the reactive power of the network at night. However, this amount of use reactive power is limited. The basic equation for power-flow analysis is derived from the nodal analysis equations for the power system: For example, for a 3-bus system,

$$\begin{bmatrix} Y_{11} & Y_{12} & Y3 \\ Y_{21} & Y_{22} & Y_{23} \\ Y_{31} & Y_{32} & Y_{33} \end{bmatrix} \begin{bmatrix} V_1 \\ V_2 \\ V_3 \end{bmatrix} = \begin{bmatrix} I_1 \\ I_2 \\ I_3 \end{bmatrix} \quad (1)$$

$$I_i = Y_{i1}V_i + Y_{i2}(V_i - V_2) + Y_{i3}(V_i - V_3) = V_i \sum_{l=1}^{n} Y_{ij} - \sum_{j=2}^{n} Y_{ij}V_j \quad j \neq i \quad (2)$$

where Y_{ij} are the elements of the bus admittance matrix V_i are the terminal voltages, and I_i are the currents supplied at each terminal. The node equation at bus i can be written as;

$$I_i = \sum_{j=1}^{n} Y_{ij}V_j \quad (3)$$

relevance between per-unit real and reactive power injected to the system at bus i and the per-unit current injected into the system at that bus:

$$P_i + jQ_i = V_i I^*_i \quad (4)$$

where V_i is the per-unit voltage at the bus; I_i* - complex conjugate of the per-unit current injected at the bus; P_i and Q_i are per-unit real and reactive powers of power system.

$$I_i = \frac{P_i - jQ_i}{V_i^*} = V_i \sum_{j=0}^{n} y_{ij} - \sum_{j=1}^{n} y_{ij}V_j \quad j \neq 1 \quad (5)$$

Inductive and capacitive operations of DG were examined to reveal the effects the voltage of feeders. During the simulation, power factor was assumed as 0.98 and fixed for Araklı-II feeder which is shown in Figure 5.

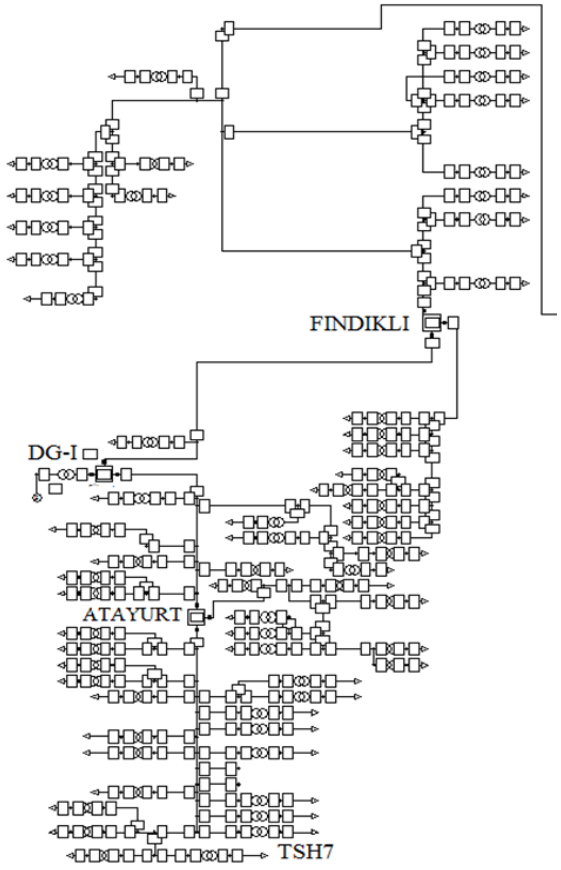

Fig. 5. Modeling of Araklı-II feeder using DIgSILENT power factory software

2.1. Voltage Profile During Night Time

Electric power demand from substation is minimum during at night. In the simulation, active power consumption is calculated as 24.5 MW at 13 January 2015 at 00:30. Consumption load values of distribution transformers are shared in proportion to the own nominal power values at feeders in the simulation. DG-I produced 6.7 MW real power and took 0.1 MVAr from network. DG-II produced 3.7 MW real power and take 0.3 MVAr from network. DGs are operated in sub-excited region at night to prevent increase of line voltage. All power values of DGs at night are shown in Table 3.

Table 3. Power values of DGs at night

DG Type	*P(MW)*	*Q(MVAr)*
DG-I	6.7	0.1
DG-II	3.7	0.3

The simulation results obtained according to this scenario are shown in Figure 6. The voltage increased at the terminal points connected to both DGs. For example, voltage of busbar rises by maximum 3% near the DG-I such as Fındıklı or Atayurt terminal.

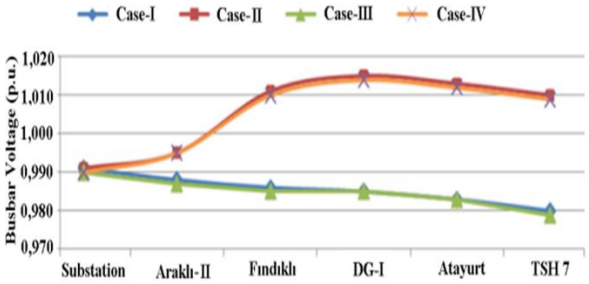

Fig. 6. Voltage profile for Araklı-II feeder at night

2.2. Voltage Profile During Peak Time

The peak power demand time of network was recorded on 29th of January 2015 at 17:30. The active power consumption is noted about 43 MW. The DGs are operated in over-excited region at peak time to prevent decrease of line voltage.

Table 4. Power values of DGs in peak time

DG	*P(MW)*	*Q(MVAr)*
DG-I	9.6	-0.4
DG-II	4.2	-0.7

2.3. Voltage Profile Estimation for Future

The average power consumption increase per year is about 5% for last decade in Turkey [10]. The peak power demand were calculated as 55 MW for the year 2020 and 70 MW for the year 2025 by using this rate. DGs are operated in over-excited region with same values in section 2.1. Terminals voltage level increased between 5% and 0.3%, approximately.

The line voltage decreases when the consumer loads increase. Adding a power transformer to the grid is a solution for this problem. However, DGs support the voltage profile and delivery power of the line in a positive way. For this reason, DGs may delay the investment to be made in this region. The voltage profile according to load estimates of 2020 and 2025 is given in Figure 7.

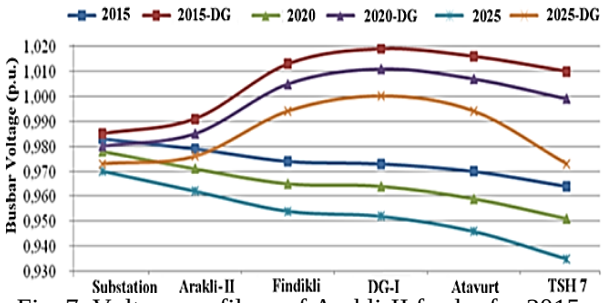

Fig. 7. Voltage profiles of Arakli-II feeder for 2015 and beyond

3. SHORT-CIRCUIT ANALYSIS

Short circuit current was occurred when two or more electrical point at different voltages contact over low impedance [11]. If it is assumed that the impedance does not change in the networks, the current value is found with the Equation 6 and 7 where;

L : Network inductance
R : Network resistance
E : Maximum value of induced voltage
V_a: Fault voltage
I_a : Fault current
Z_f : Fault impedance
θ, ϕ: Phase angle
a : Operator
I_{max}: Maximum current value
$I_{0, 1, 2}$: Current symmetrical components
$Z_{0, 1, 2}$: Impedance symmetrical components

$$L\frac{di}{dt}+Ri=E_m\sin(\omega t+\theta) \quad (6)$$

$$i=I_m\sin(\omega t+\theta-\phi)-I_m\sin(\theta-\phi)e^{-Rt/L} \quad (7)$$

The short circuit current consists of AC and DC components. While the AC component is a continuous signal that varies according to the frequency, the dc component t '= L / R is a current that goes out according to the time constant.

$$i=I_m\sin\omega t+I_{dc}e^{-Rt/L} \quad (8)$$

In the phase-to-earth short circuit, the current value can be found with the help of the following equations with the help of symmetrical components.

$$\begin{vmatrix}I_0\\I_1\\I_2\end{vmatrix}=\frac{1}{3}\begin{vmatrix}1&1&1\\1&a&a^2\\1&a^2&a\end{vmatrix}\begin{vmatrix}I_a\\0\\0\end{vmatrix}=\frac{1}{3}\begin{vmatrix}I_a\\I_a\\I_a\end{vmatrix} \quad (9)$$

The total phase a current for a line-to-ground fault equals three times the phase a positive sequence current.

$$I_0=I_1=I_2=\frac{1}{3}I_a \quad (10)$$

If the phase-to-ground short-circuit current is over the Z_F resistance, the short-circuit current value is;

$$3I_0Z_f=V_0+V_1+V_2=-I_0Z_0+(V_a-I_1Z_1)-I_2Z_2 \quad (11)$$

$$I_a=3I_0=\frac{3V_a}{(Z_1+Z_2+Z_0)+3Z_f} \quad (12)$$

In this simulation, single phase ground and three phase steady-state short circuit currents (Ik") were calculated per IEC60909 standard. Short-circuit faults were performed on high and medium voltage (MV) busbar of substation, and on some important connecting nodes at Araklı-II feeder.

3.1 Phase-to-Ground Short Circuit Analysis

Most of the short-circuit failures in medium voltage network is phase-to-ground [12]. The most important factor on the short-circuit current is the short-circuit power of grid and short-circuit impedance [13]. Although short circuit impedance is high in single-phase short-circuit and it is low in three-phase short-circuit. Short relative circuit voltage value (U_k %) of power transformers is shown in Table 5. Single-phase short-circuit current and effects of DGs on this current shown in Table 6. These currents values were investigated for all operation conditions when generator was producing maximum power.

DGs caused very little current rise at substation cabin. But they highly affected busbar and cabins which are close to them. It is observed that phase-to-ground short circuit fault current increased 13.5% at busbar which is close to DG-I and increased 1.21% at MV busbar on substation.

Table 5. Information of distribution transformers

Power (KVA)	Short-circuit Voltage (%)	X/R	Vector Group	Earth Resistance(Ω)
TR-A	9.12	20	YNyn0	20
TR-B	12.3	50	YNyn0	50
2500	6	6.17	Dyn11	-/0
2000	6	5.62	Dyn11	-/0
1600	6	5.55	Dyn11	-/0
1250	6	5.68	Dyn11	-/0
1000	6	5.63	Dyn11	-/0
800	6	5.42	Dyn11	-/0
630	4.5	4.14	Dyn11	-/0
400	4.5	3.53	Dyn11	-/0
250	4.5	3.05	Dyn11	-/0
160	4.5	2.64	Yzn11	-/0
100	4.5	2.08	Yzn11	-/0
50	4.5	1.49	Yzn11	-/0

3.2 Three-Phase Short Circuit Analysis

In electrical systems, three-phase short circuit current occurs maximum 5% of all short circuit failure [14]. This fault current is symmetrical and its value is very high [15]. It was observed that the three phase short-circuit currents of the bus bars decreases with the distance from substation. The effect of DGs on the three-phase short-circuit current is relatively low at the terminals near the substation. However, this fault current increase is very high in the terminals where the DGs are connected. At the end of analyses, it was determined that three-phase fault current increased 28.2% at terminal which is close to DG-I and 10.7% at substation terminals. Three-phase short circuit currents of Araklı- II feeder and effects of DGs shown in Table 7.

Table 6. Phase-to-Ground short circuit currents (kA)

Feeder	DG (No)	DG- I	Change (%)	DG-II	Change (%)	DG I-II	Change (%)
TM-HV	8.94	9.02	0.92	9.00	0.70	9.08	1.57
TM-MV	3.73	3.76	0.67	3.75	0.56	3.78	1.21
Araklı	2.89	2.99	3.18	2.91	0.52	3.00	3.59
Fındıklı	1.94	2.14	10.58	1.94	0.36	2.15	10.79
DG-I	1.78	2.02	13.29	1.79	0.34	2.02	13.46
Atayurt	1.04	1.12	6.99	1.05	0.19	1.12	7.18
TSH-7	0.36	0.37	2.23	0.36	0.00	0.37	2.23

Table 7. Three phase short circuit currents (kA)

Feeder	DG (No)	DG I	Change (%)	DG-II	Change (%)	DG I-II	Change (%)
TM-HV	8.90	9.03	1.44	9.00	1.09	9.12	2.44
TM-MV	10.59	11.24	6.13	11.08	4.62	11.73	10.75
Araklı	6.13	6.80	10.90	6.28	2.40	6.94	13.27
Fındıklı	2.85	3.52	23.56	2.88	0.95	3.55	24.44
DG-I	2.47	3.15	27.51	2.49	0.81	3.17	28.24
Atayurt	1.55	1.81	17.04	1.56	0.45	1.82	17.30
TSH-7	0.48	0.50	5.05	0.48	0.00	0.50	5.05

4. CONCLUSION

The effect of distributed generations on voltage profile, single-phase to ground and three-phase short circuit currents were investigated in this study. The following conclusions can be summary as;

- When distributed generations is operated in sub-excited region, voltage profile increase 3% at busbar which close to distributed generation -I but voltage decrease 0.1% at substation centers.
- When distributed generations is operated in over-excited region, voltage profile increase 5% at busbar which is close to distributed generation -I and 0.3% at substation centers.
- Voltage levels increase from 0.935 p.u. to 0.973 p.u. at end of Araklı-II feeder when distributed generations are operated in over-excited region voltage.
- By providing active power from distributed generations to the grid, power transformer-A loading decreased from 119% to 96% and power transformer-B loading decreased from 88% to 71%.
- When distributed generations operated, Araklı-II distribution line loading was reduced by 33%.
- Phase-to-ground short circuit fault current increase is 13.46% and three phase short circuit current increase obtained as 28.2% at busbar which is close to distributed generation-I. So, distributed generations is more effective in three-phase short circuit fault current then phase-to-ground short circuit fault current.
- Phase-to-ground short circuit fault current increases 1.2% and three phase short circuit fault current increases 10.7 % at substation centers.

References

[1] F.W. Pickard, Massive electricity storage for a developed economy of ten billion people, IEEE Access 3: 1392-1407, (2015).

[2] M. Altin, E. U. Oguz, E. Bizkevelci, and B. Simsek, Distributed generation hosting capacity calculation of MV distribution feeders in Turkey, In Innovative Smart Grid Technologies Conference Europe (ISGT-Europe), IEEE PES 1-7, (2014).

[3] T. Ackermann, G. Anderson, and L. Soder, Distributed Generation, A Definition, Electric Power Systems Research, 57, 195-204, (2000).

[4] F. M. Nuroğlu, and A.B. Arsoy, Voltage profile and short circuit analysis in distribution systems with DG, Electric Power Conference, (2005).

[5] F. M. Nuroğlu, and A. B. Arsoy, Central coordination relay for distribution systems with distributed generation, Turkish Journal of Electrical Engineering and Computer Sciences, 23, 2150-2160, (2015).

[6] L. Bam, and W. Jewell, Power system analysis software tools, In Power Engineering Society General Meeting, IEEE 139-144, (2005).

[7] Single-line diagram of Arsin substation, TEIAS (Turkish Electricity Transmission Company), http://www.teias.gov.tr (Last access date: 11/04/2016).

[8] P. P. Barker, and R.W. De Mello, Determining the impact of distributed generation on power systems. I. Radial distribution systems. In Power Engineering Society Summer Meeting, IEEE, Vol. 3, 1645-1656, (2000).

[9] R. A. Walling, R. Saint, R. C. Dugan, Summary of Distributed Resources Impact on Power Delivery Systems, IEEE Trans. on Power Systems, 23(3), 1636-1644, (2008).

[10] A. Yücekaya, Evaluating the Electricity Supply in Turkey Under Economic Growth and Increasing Electricity Demand, Journal of Engineering Technology and Applied Sciences, 2(2), 81-89, (2017)

[11] D. Sweeting, Applying IEC 60909, fault current calculations, IEEE Transactions on Industry Applications, 48(2), 575-580, (2012).

[12] R. Fediuk, Limitation of the single-phase grounding current. In Mechanical Engineering, Automation and Control Systems International Conference on IEEE, 1-4, (2014).

[13] X. Liu, H. Chen, Y. Tao, and C. Huqian, Short-circuit current limiting for ring distributed power

system integrated with multiple sources, In PES General Meeting| Conference & Exposition, 2014 IEEE,1-5, (2014).
[14] Schneider Electric Company, Calculation of short-circuit currents, Cahier technique no. 158, (2005).
[15] D. Dufournet, and G. Montillet, Three-phase short circuit testing of high-voltage circuit breakers using synthetic circuits. IEEE transactions on power delivery, 15(1), 142-147, (2000).

Biographies

Alkan AKSOY was born in, 1980 in Trabzon, Turkey. He received his B.Sc. and M.Sc. degrees in Electrical & Electronics Engineering from Karadeniz Technical University (KTU) in Trabzon, Turkey, in 2003 and 2016 respectively. He is currently a lecturer in Electricity and Energy Department, Sürmene Abdullah Kanca Vocational School of KTU, and Ph.D student at Atatürk University. His research interests include power system modeling and analysis, distributed generation and illumination systems.

E-mail: alkanaksoy@ktu.edu.tr

Fatih Mehmet NUROĞLU received his B.Sc. degree from Istanbul Technical University Turkey, in 1992, and the M.S. degree from the Pennsylvania State University, Philadelphia, PA, USA in 1997, and the Ph.D. degree from Kocaeli University, Turkey in 2011. He is currently an Assistant Professor at Karadeniz Technical University, Trabzon, Turkey. His research interests include power system modeling and analysis, power system protection, and distributed generation.

E-mail: fmn@ktu.edu.tr